SPICE

Sentinel-3 Performance improvement for ICE sheets

Scientific Review Technical Note

Scientific Exploitation of Operational Missions (SEOM)

Sentinel-3 SAR Altimetry

Study 4: Ice Sheets

Prepared by :	Malcolm McMillan	date: 19/11/2015
Approved by :		date:

Change Log

Issue	Author	Affected Section	Reason	Status
1.1	Malcolm McMillan	All	Document structure created.	Released to consortium 23/10/2015.
1.2	Malcolm McMillan	All	Document created.	Released to consortium 16/11/2015.
1.3	SPICE team	All	Document updated.	Released to ESA 19/11/2015.

Distribution List

Jerome Benveniste	ESA
Marco Restano	ESA
Americo Ambrozio	ESA
Malcolm McMillan	University of Leeds
Andrew Shepherd	University of Leeds
Mònica Roca	isardSAT
Maria Jose Escorihuela	isardSAT
Roger Escolà	isardSAT
Pierre Thibaut	CLS
Frédérique Rémy	LEGOS

Document Status:

Internal

Contents

List of Figures

Acronyms and Abbreviations

AD	Applicable Documents
AIS	Antarctic Ice Sheet
ATBD	Algorithm Theoretical Basis Document
ATM	Airborne Topographic Mapper
CLS	Collecte Localisation Satellites

CNES	Centre National d'Etudes Spatiales
DDP	Delay Doppler Processor
DPM	Detailed Processing Model
ERS	European Remote Sensing Satellite
ESA	European Space Agency
FBR	Full Bit Rate
GEOS	Geodynamics and Earth Ocean Satellite
GIS	Greenland Ice Sheet
ITT	Invitation To Tender
KO	Kick off meeting
LEGOS	Laboratoire d'Etudes en Géophysique et Océanographie Spatiales
LRM	Low Resolution Mode
NASA	National Aeronautics and Space Administration
NSIDC	National Snow and Ice Data Center
OCOG	Offset Centre Of Gravity
pLRM	Pseudo-LRM
POCA	Point Of Closest Approach
PRF	Pulse Repetition Frequency
RB	Requirements Baseline document
RDSAR	Reduced SAR (also known as Pseudo-LRM)
SAR	Synthetic Aperture Radar
SARin	Synthetic Aperture Radar interferometric
SEOM	Scientific Exploitation of Operational Missions
SoW	Statement Of Work
SPICE	Sentinel-3 Performance improvement for Ice sheets
SR	Science Review
STM	Sentinel-3 Surface Topography Mission
SWH	Significant Wave Hieght

TP	Technical Proposal
UL	University of Leeds
WP	Work Package

Applicable Documents

AD1	Scientific Exploitation of Operational Missions (SEOM). Sentinel-3 SAR Altimetry Statement of Work (SEOM S3-4SCI SAR Altimetry). Issue 1, 27/09/2014.
AD2	Special Conditions of Tender. Appendix 4 to AO/1-8080/14/I-BG.
AD3	SPICE Technical Proposal.
AD4	SPICE Implementation Proposal.
AD5	SPICE Requirements Baseline document.

Table 1. Applicable Documents.

1. Introduction

1.1. Purpose

This document comprises the Scientific Review Technical Note for the Sentinel-3 Performance improvement for ICE sheets (SPICE) proposal, which is a response to the European Space Agencies (ESA's) Sentinel 3 For Science – SAR Altimetry Studies (S3 4 SCI – SAR Altimetry Studies) Invitation To Tender (ITT), Ref. AO/1-8080/I-BG. SPICE addresses the Study 4 theme related to Ice Sheets. The Science Review has been written by the University of Leeds (UL), with contributions from isardSAT, CLS and LEGOS. UL as the prime contractor is the contact point for all communications regarding this document.

Address:

School of Earth and Environment,

Maths/Earth and Environment Building,

The University of Leeds,

Leeds,

LS2 9JT,

UK

Att: Malcolm McMillan (Science Lead)

Email: m.mcmillan@leeds.ac.uk

Telephone: + 44(0) 113 34 39085

Fax: +44 113 343 5259

ESA Bidder Code: 6000012896

1.2. Science Review structure

The aim of the Scientific Review Technical Note is to provide a critical review of the state of the art methods and algorithms relevant to the SPICE project. That is, to undertake a review of the scientific literature related to conventional (pulse-limited) and Synthetic Aperture Radar (SAR) altimetry measurement of ice sheets. To achieve this aim, the document will give an overview of all scientific aspects relevant to the SPICE project, structured into the following sections:

- **Section 2 –** An overview of the scientific context and motivation for the SPICE study.
- **Section 3** – A detailed overview of conventional altimetry observation of ice sheets.
- **Section 4** – A detailed overview of Synthetic Aperture Radar altimetry.
- **Section 5** – A summary of recommendations for the SPICE project.

2. Scientific Background

It is fifty years since the concept of mapping ice sheet topography using satellite altimetry was first proposed [*Robin*, 1966]. Since then, this vision has become a reality, as a succession of satellite radar altimeters have acquired measurements across Earth's polar regions, and resolved the ice sheets of Greenland and Antarctica at the continental scale (Figure 1). During this time, measurement accuracy has improved by orders of magnitude, and satellites have been launched into orbits with higher inclinations, providing greater coverage of the ice sheets. From the first glimpse of the southern tip of the Greenland Ice Sheet offered by GEOS-3 during the 1970's, satellite observations have progressed to increasingly higher latitudes, notably with Seasat (72.2°), ERS-1/2 (81.5°) and most recently CryoSat-2 (88°). These measurements have, over the last quarter of a century, provided a near-continuous record of ice sheet elevation and elevation change [*Wingham et al.*, 1998; *Davis et al.*, 2005; *Shepherd and Wingham*, 2007; *Zwally et al.*, 2011; *Flament and Rémy*, 2012; *McMillan et al.*, 2014]. In doing so, they have transformed our ability to monitor the great ice sheets, and fostered a new understanding of both the speed and manner in which they change.

As with all geodetic datasets, conventional radar altimeters have their own intrinsic strengths and weaknesses. The recent realisation of Delay-Doppler, or SAR, altimetry by CryoSat-2 has demonstrated the potential to address some of these existing challenges and represents possibly the most significant technical advance in radar altimetry for several decades. The launch of Sentinel-3, now a global SAR mission, will therefore complete the transition, started by CryoSat-2, to a new era of SAR altimetry over ice sheets. This promises new advances in our capacity to monitor the changing nature of these polar regions and provides the scientific motivation for the SPICE project. To begin the Scientific Review, we briefly outline the scientific context for the SPICE study, by summarising ice sheet evolution during the satellite era. This forms the scientific and societal motivation for SAR altimetry observation of ice sheets.

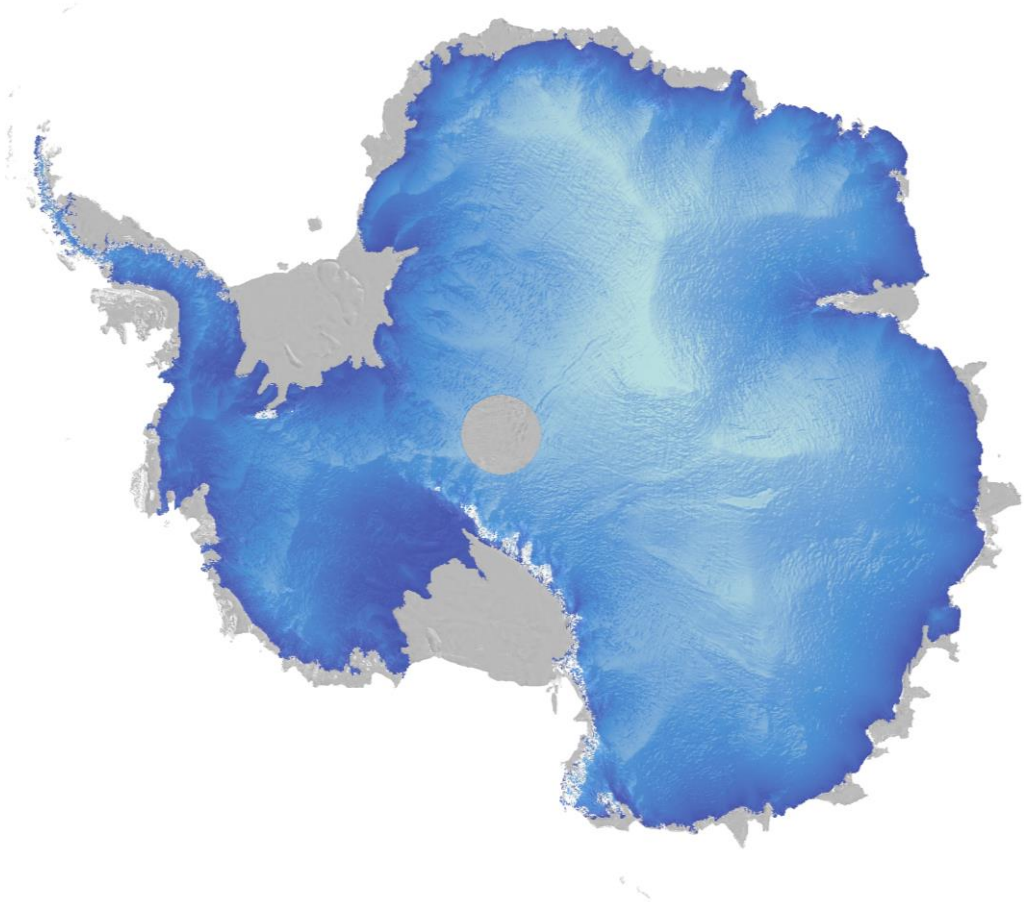

Figure 1. Shaded relief of Antarctic Ice Sheet surface topography, derived from CryoSat-2 observations.

2.1. Greenland Ice Sheet Evolution during the Satellite Era

During the last two decades, the Greenland Ice Sheet has shifted from a state of near balance, to one of significant mass loss [*Rignot et al.*, 2011; *van den Broeke et al.*, 2011; *Shepherd et al.*, 2012; *Vaughan et al.*, 2013]. Recent estimates found that between 1992 and 2001, the average rate of ice loss from Greenland was 34 ± 40 Gt yr^{-1} [*Vaughan et al.*, 2013]. Over the following decade, the rate of ice loss accelerated substantially (Figure 2), to reach an average of 215 ± 59 Gt yr^{-1} between 2002 and 2011 [*Vaughan et al.*, 2013]. Since then the rate of mass loss has increased further still [*Schrama et al.*, 2014]. Total ice losses from Greenland equate to approximately 10% of the measured global sea level rise during the last two decades [*Church et al.*, 2013].

Changes in Greenland ice mass are primarily linked to two processes; changing surface mass balance, for example from increased melting or accumulation, and variable glacier flow, which affects the quantity of ice lost to the ocean. The mass imbalance observed during the 2000's [*van den Broeke et al.*, 2011; *Shepherd et al.*, 2012; *Vaughan et al.*, 2013] was caused, in roughly equal parts, by decreased surface mass balance and increased ice discharge [*van den Broeke et al.*, 2009]. The decreased surface mass balance was primarily due to higher rates of surface melting [*van den Broeke et al.*, 2009], caused by warmer summer temperatures across the ice sheet. This resulted from a combination of global temperature increases and shifting patterns of regional atmospheric circulation [*Hanna et al.*, 2008; *Fettweis et al.*, 2011; *Bindoff et al.*, 2013]. The causes for changes in ice discharge are less certain, because of the complex nature of ice-ocean interactions and the numerous processes that can induce and modulate a dynamic response [*Joughin et al.*, 2012]. There is, however, evidence that a greater influx of warm ocean water occurred in some regions at the time of glacier acceleration [*Holland et al.*, 2008; *Rignot et al.*, 2010], although a direct causal link to ice dynamical change has yet to be definitively established.

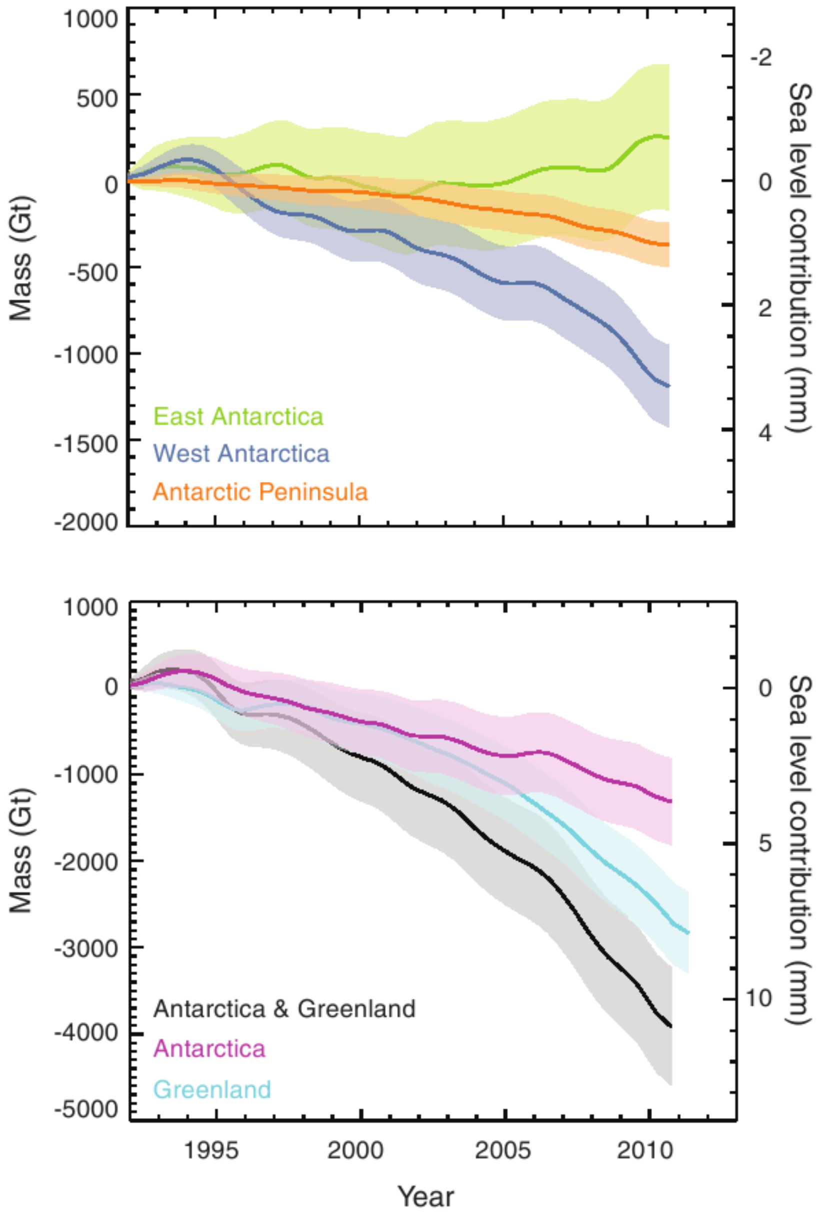

Figure 2. Ice sheet contribution to sea level during the era of systematic satellite observation, from Shepherd et al. (2012).

2.2. Antarctic Ice Sheet Evolution during the Satellite Era

In Antarctica, satellite data acquired over the last two decades have shown that the ice sheet lost mass at an average rate of 88 ± 35 Gt yr^{-1} [*Vaughan et al.*, 2013]. During that period, ice losses have increased with time (Figure 2), from a rate of 30 ± 67 Gt yr^{-1} (1992-2001) to 147 ± 75 Gt yr^{-1} (2002-2011). Because of the cold climate, the ice sheet experiences relatively little surface melting by the atmosphere, with the exception of parts of the Antarctic Peninsula. Instead, Antarctic mass balance is dominated by ice loss to the ocean, which is offset by inland snowfall accumulation. Satellite observations have revealed a wide range of behaviour across this vast continent (Figure 3), which is briefly summarised in the following sections.

In West Antarctic, the most rapid changes have been observed across the Amundsen Sea Sector. Between 2005 and 2010, the mass imbalance of this region alone contributed annually 0.28 ± 0.05 mm to sea level [*Shepherd et al.*, 2012], equivalent to almost 10% of the observed rate of global sea level rise [*Church et al.*, 2013]. The largest glaciers in this region have undergone substantial flow acceleration in recent decades. Ice discharge into the ocean along this coastline has increased by 77% since the 1970's [*Mouginot et al.*, 2014], leading to substantial ice loss in this region, which has manifested itself as widespread ice sheet thinning [*Shepherd et al.*, 2002; *Zwally et al.*, 2005; *Pritchard et al.*, 2009; *Helm et al.*, 2014; *McMillan et al.*, 2014] and grounding line retreat [*Rignot*, 1998; *Park et al.*, 2013; *Rignot et al.*, 2014]. Since the early 1990's, these glaciers have retreated up to 35 km inland [*Joughin et al.*, 2010; *Park et al.*, 2013; *Rignot et al.*, 2014], raising questions about the future stability of this part of Antarctica.

In East Antarctica, the ice sheet has been broadly in balance over the last two decades [*Shepherd et al.*, 2012]. The most notable changes have been caused by a series of extreme accumulation events that deposited several hundred gigatonnes of snow in Dronning Maud Land between 2009 and 2011 [*Boening et al.*, 2012; *Shepherd et al.*, 2012; *Lenaerts et al.*, 2013; *McMillan et al.*, 2014], and the sustained near-terminus thinning of the Totten Glacier, which discharges the largest volume of ice of all glaciers in East Antarctica [*Rignot and Thomas*, 2002].

The Antarctic Peninsula has been one of the fastest warming regions of Earth during the latter half of the twentieth century. Alongside rising air temperatures [*Turner et al.*, 2005], there is also evidence of increasing ocean temperatures in recent decades [*Robertson et al.*, 2002; *Martinson et al.*, 2008]. Substantial glaciological changes have occurred across this region, particularly near to the coast, where fast flowing glaciers feed numerous small ice shelves. Many of these ice shelves have undergone thinning and retreat [*Shepherd et al.*, 2003, 2010; *Cook and Vaughan*, 2010; *Pritchard et al.*, 2012], and in some cases have disintegrated entirely [*Rott et al.*, 1996; *Scambos et al.*, 2000; *Humbert et al.*, 2010], This in turn, has triggered sustained acceleration and mass loss from their tributary glaciers [*Rignot et al.*, 2004, 2005; *Rott et al.*, 2011].

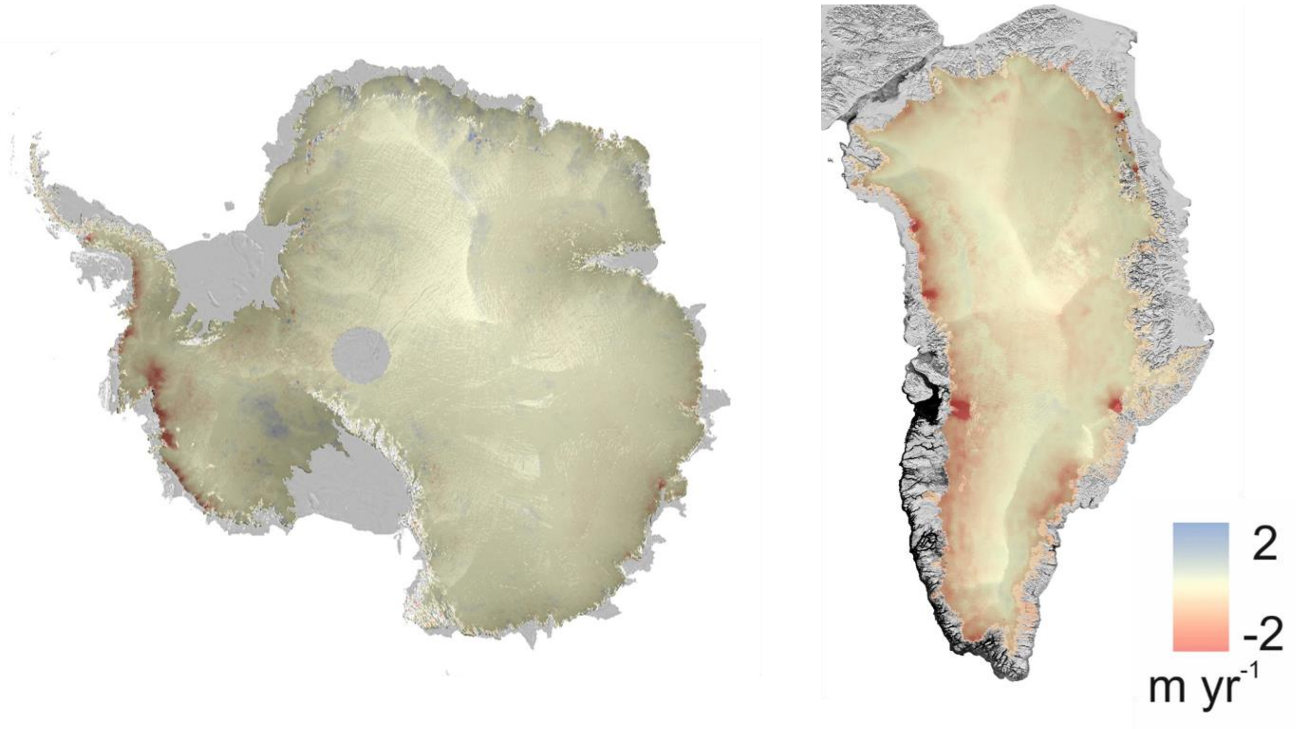

Figure 3. Rate of surface elevation change of the Antarctic and Greenland Ice Sheets between 2010 and 2014 from CryoSat-2 radar altimetry.

The satellite record acquired over the past two decades has demonstrated the complexity of ice sheet change and the global impact that these changes can have, through the loss of ice to the ocean. They have also highlighted the challenges associated with making centennial scale projections of future ice sheet evolution and the need to develop long-term, systematic monitoring programmes to further extend the current satellite record. Critically, ice mass balance needs to be resolved at the scale of individual glacier catchments, and with regular temporal sampling, so as to develop the process-based understanding required for developing realistic physical models. Radar altimetry, with its regular repeat cycle and moderate spatial resolution, is well suited to this task. This concludes the brief overview of the scientific context for the current project. In the following sections we provide detailed reviews of conventional and SAR altimetry, focusing on key aspects relevant to ice sheet observations and the SPICE study.

3. Conventional Altimetry

3.1. Conventional Altimetry Introduction

Satellite radar altimeters are nadir-pointing active microwave instruments. For polar Earth observation, operating at microwave frequencies is particularly beneficial, since it enables largely uninterrupted data acquisition because the signal can penetrate cloud cover and operation is independent of solar illumination. Conventional polar altimeter missions have tended to operate with a frequent, usually monthly, repeat cycle, meaning that regular temporal sampling of the same ground location is achieved. This is beneficial for systematic monitoring of the specific ice sheet regions covered by the satellite ground tracks, albeit at the expense of less comprehensive spatial sampling.

For our purposes, we define conventional altimeters as those that process echoes on a pulse-by-pulse basis, using a relatively low pulse repetition frequency (PRF) and incoherent averaging of the detected echoes to reduce the impacts of radar speckle and instrument noise. This mode of operation is to be contrasted with Synthetic Aperture Radar (SAR), or Delay-Doppler, altimetry, which utilises a much higher PRF and coherent processing of bursts in order to improve azimuth resolution. SAR altimetry is addressed in detail in Section 4. With the exception of CryoSat-2, all polar orbiting satellite altimeters to date have operated conventional instruments, including ERS-1, ERS-2, Envisat and SARAL. The footprint of these instruments is entirely pulse-limited and this mode of operation is commonly referred to as a pulse-limited, low resolution or low rate mode (LRM).

The following sections are designed to give a brief overview of the key characteristics and processes related to conventional altimetry, with a focus on ice sheet observation. First we summarise some of the relevant characteristics of the conventional altimeter system, before going on to review some of the key processes relevant to making ice sheet elevation measurements. Following this, we provide an overview of the principle methods for estimating ice sheet elevation change. The existing literature on these topics is extensive and for more detailed descriptions of any of the topics discussed we refer the reader to one of the many comprehensive compilations and textbooks, for example *Fu and Cazenave* [2001].

3.2. Characteristics of Conventional Altimeter Systems

Radar altimeters operate by transmitting short pulses of microwave radiation, recording the backscattered reflection from Earth's surface, and computing the corresponding range based upon the travel time of the pulse. Given precise orbit and range information, the surface elevation above a reference datum can be computed. In practice, various corrections must be applied to account for factors such as the lag of the on-board tracker and the varying atmospheric delays encountered by the echo as it travels between the satellite and Earth's surface.

Satellite altimeters have relatively narrow antenna beam widths, typically around 1°, which from an orbital altitude of ~ 800 km, illuminate a ~ 16 km diameter footprint on the ground. Although this so-called beam-limited footprint is relatively large, much finer ground resolution is achieved because it is determined not by the beam-illuminated area, but by the duration of the emitted microwave pulse. More specifically, the ground resolution of a conventional pulse-limited altimeter is given by the pulse-limited footprint, which is defined as the maximum area from which radar backscattering is simultaneously received, prior to the trailing edge of the pulse intersecting the surface (Figure 4). The pulse limited footprint of radar altimeters is typically ~ 2 km diameter over a flat surface.

3.3. Principles of Measuring Ice Sheet Surface Elevation

A satellite altimeter emits a pulse of electromagnetic radiation and records the reflected signal. Because the surface elevation, and hence travel time, is not known precisely, the instrument is set to receive over a fixed 'analysis window'. This window is positioned according to the on-board tracker, a predictive device whose purpose is to ensure that the echo reflected from Earth's surface stays within the window. To achieve this, on-board trackers are either guided by preceding echoes (closed-loop tracking) or use pre-existing information about the surface elevation (open-loop tracking). Within the analysis window, the altimeter records the distribution, with time, of the power reflected from Earth's surface, accumulated within a number of range bins, or gates, which span the window. This power distribution, or 'waveform', provides precise information on both the range to, and properties of, the illuminated surface. In an idealised sense, waveforms have a characteristic shape (Figure 4).

Over a non-penetrating surface, the leading edge of the waveform corresponds to the expanding area intersected by the radar pulse and the illuminated surface within the pulse-limited footprint. When the wavefront first meets the surface, the footprint begins as a point. The area illuminated by the pulse then grows until the trailing edge of the wavefront intersects the surface. The pulse-limited footprint is the area at this time, and is defined in terms of the diameter of the leading edge of the pulse when the trailing edge of the pulse first breaks the surface. At the point when the trailing edge intersects the surface, the waveform reaches its peak power and thereafter it begins to decay. The illuminated area is now an annulus, which progressively spreads out from the pulse limited footprint towards the edge of the beam footprint. Although the annulus area remains constant, the reflected power decreases according to the antenna pattern. This process is illustrated in Figure 4.

The waveform not only provides precise ranging information but also details of the scattering properties of the surface. In the case of the ocean, where the surface is homogeneous, the height distribution of scatterers is the main factor which determines the detected echo shape. In the case of an ice sheet, however, in addition to more irregular topographic effects, the snowpack characteristics will affect the waveform shape, with roughness, density and water content all influencing the radar wave interaction with the snowpack, and therefore the power distribution of the reflected echo. These issues will be addressed in more detail in the following section.

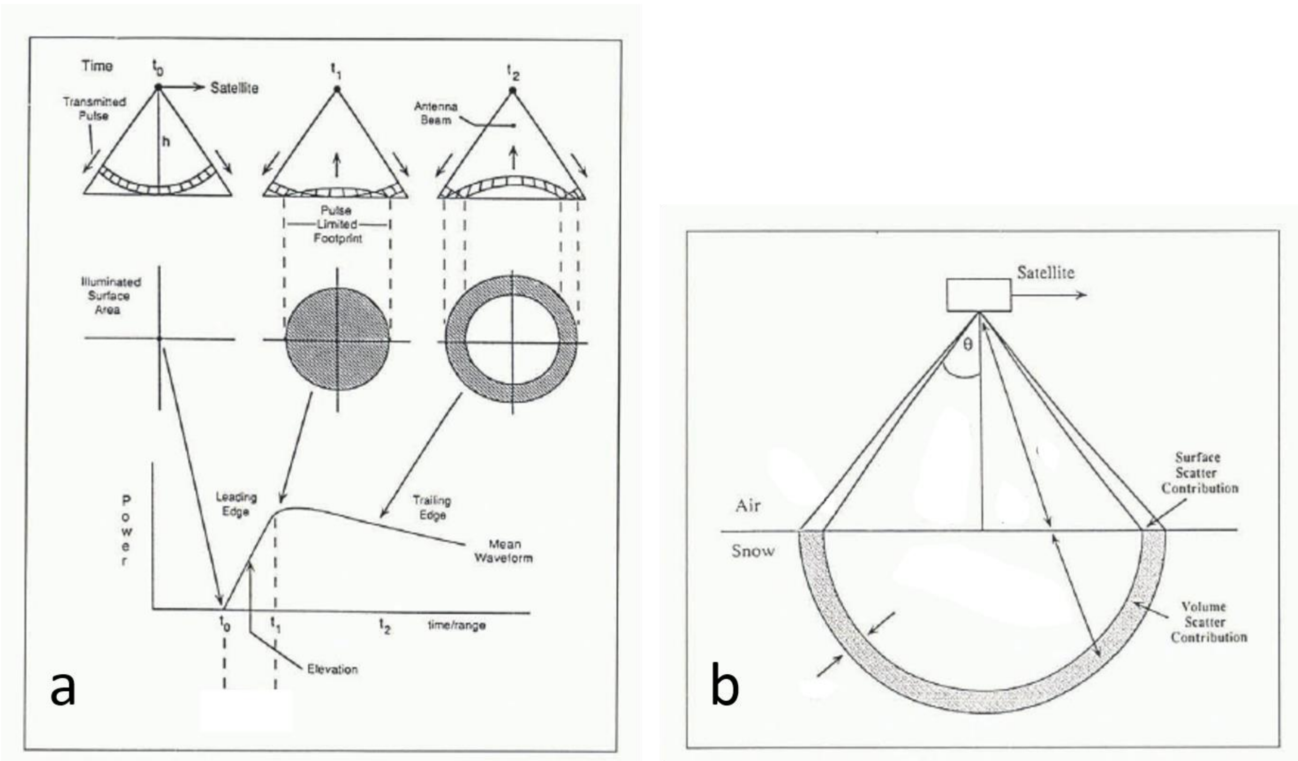

Figure 4. Illustration of the imaging geometry of a nadir pointing radar altimeter. (a), side and plan views with no volume scattering, and correspondence to waveform shape, (b) side view with volume scattering, adapted from *Davis and Moore* [1993].

To retrieve precise measurement of range, and hence elevation from the detected waveform, the process of retracking is used. This procedure effectively corrects for the misalignment of the waveform relative to the nominal tracking point of the analysis window. After retracking, the range to the reference point of the analysis widow is added to the epoch retrieved from retracking, to determine a precise estimate of the range to the illuminated surface. Then, given knowledge of the satellite altitude and attitude, the range can be used to compute the surface elevation.

3.3.1. Retracking Methods

Retracking is a critical step for determining reliable measurements of ice sheet elevation. As a result, considerable literature has been generated on the subject and many different ice sheet retrackers have been developed [*Martin et al.*, 1983; *Bamber*, 1994; *Davis*, 1997; *Wingham et al.*, 1998; *Legresy et al.*, 2005; *Helm et al.*, 2014]. Retracking involves fitting a model, of varying complexity, to the detected waveform, and attempting to retrieve a stable point on that waveform which relates to some aspect of the illuminated surface elevation.

Retrackers can be broadly categorised according to whether they employ an empirically-based or physically-based formulation. The former fit a model which is purely empirical in its form, whereas the latter have, as their basis, the physical theory which describes the theoretical radar pulse interaction with the scattering surface. Here we focus on conventional altimetry retracking algorithms, with SAR retracking covered in Section 4.3.

Over ocean surfaces, the theoretical radar response can be described by the Brown-Hayne ocean model [*Brown*, 1977; *Hayne*, 1980], which convolves the flat sea surface response, the radar point target response, and the elevation probability density function of surface scatterers. Physically-based ocean retrackers use this theoretical formulation as the basis for the waveform model that is used to retrieve the ocean surface elevation.

Over ice sheet surfaces, the theoretical response is complicated by the influence of more irregular topography and the penetration of the radar pulse into the snowpack [*Ridley and Partington*, 1988]. Figure 5 provides an example of the complex nature of waveforms retrieved over an irregular topographic surface, in this case a 70 metre depression in the ice surface caused by a drained subglacial lake. These data have been acquired in interferometric mode, allowing the echoes to be precisely located in the across track plane and greater detail to be resolved than would be possible with non-interferometric altimetry. As the altimeter beam illuminates this feature, multiple coherent peaks are formed in the detected waveforms, which correspond to reflections from distinct surfaces within the beam footprint that are orthogonal to the direction of wave travel. These relate to scattering from both the base and the rim of the depression. This example demonstrates the complexity of ice sheet waveforms and the challenges associated with trying to adequately account for this within a theoretical waveform model.

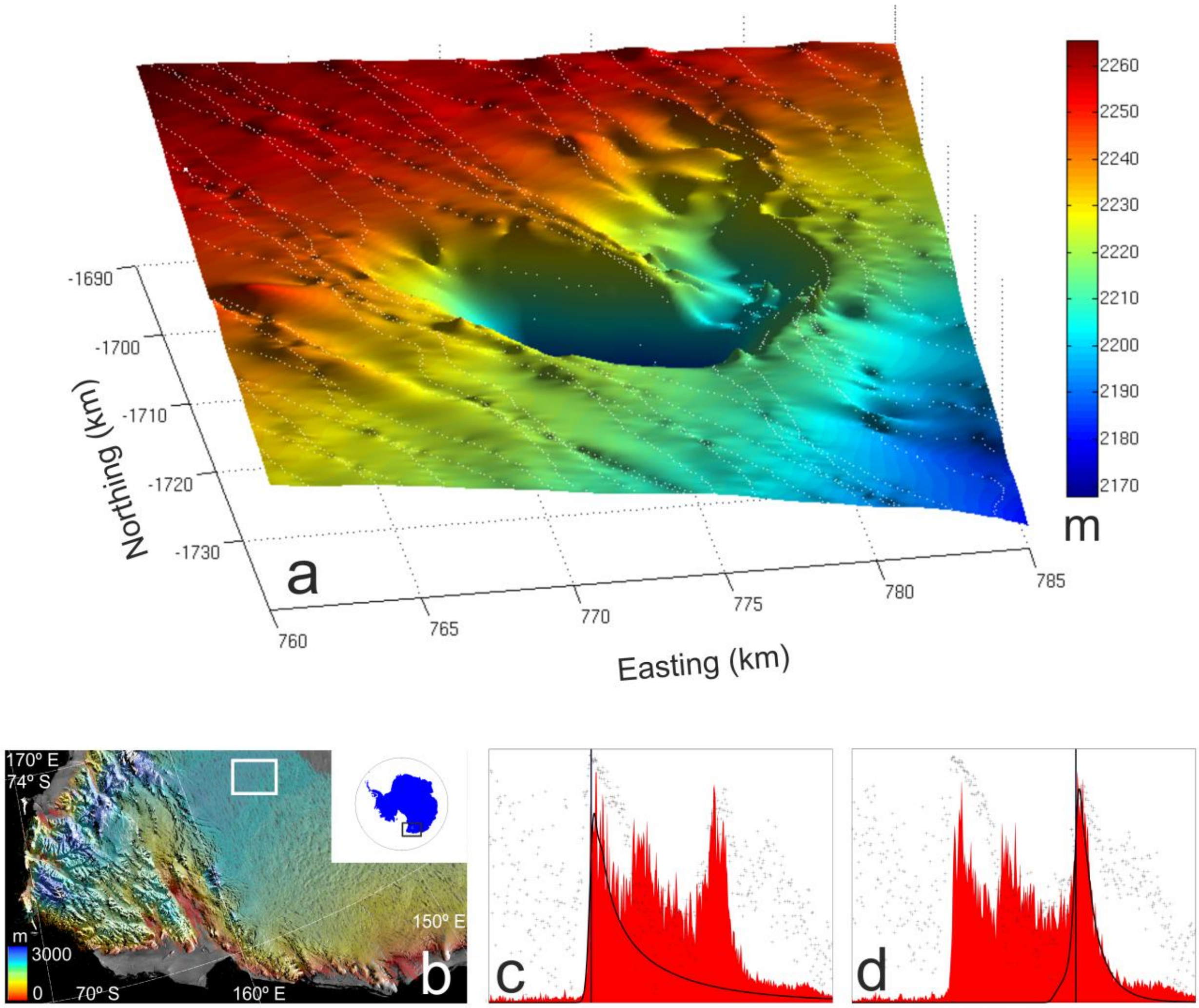

Figure 5. a. Surface expression of a drained subglacial lake, mapped by CryoSat-2 interferometric mode data (white dots) acquired between January and November 2011. b. Location of the subglacial lake, coloured tracks are CryoSat-2 SARin elevation measurements. c and d. Power (red) and coherence (black dots) of two consecutive 20 Hz SARin mode echoes, where the retracker switched from the rim (c) to the bottom (d) of the surface depression. The black curve shows the retracker fit to the echo power and the vertical black line marks the retracking point used to determine elevation, from *McMillan et al.* [2013].

Over ice sheets, these complicating factors mean that it cannot be assumed that the pulse limited footprint is centred at nadir. It is also clear that the elevation probability density function is not well resolved, because of both unknown surface topography and the scattering distribution with depth. The latter distribution is challenging to determine and can vary spatially, temporally and with viewing geometry, depending upon the particular scattering characteristics of the snowpack. This, in turn, can alter the shape of the detected waveform. For example, the width of the leading edge can be affected both by surface roughness and subsurface backscattering [*Legresy and Remy*, 1997], and the trailing slope is affected by longer-wavelength roughness and the ratio of surface to volume backscatter [*Remy et al.*, 2001].

As a result of these complicating factors, although some closed-form analytic descriptions for ice sheets have been developed [*Davis and Moore*, 1993], empirical retrackers are most commonly used. These aim to provide a stable solution which is relatively insensitive to distortions in the waveform shape caused by surface topography and effects linked to snowpack characteristics. Several different formulations of empirical retrackers have been developed for the purpose of ice sheet observation, including the Offset Centre Of Gravity retracker [*Wingham*, 1995; *Wingham et al.*, 1998], threshold retrackers [*Davis*, 1997; *Helm et al.*, 2014; *Gray et al.*, 2015; *Nilsson et al.*, 2015] and the β-parameter retracker [*Martin et al.*, 1983]. It is worth noting that the latter, whilst based on an empirical formulation, does show some similarity to the theoretical shape of the Brown-Hayne model.

In the context of ice sheet altimetry, there is presently no clear optimal choice of retracker. This subject is still an open area of research and debate, and the choice is likely to depend upon the purpose of the study. Choosing a threshold retracker for example, which retracks low on the leading edge, would be expected to minimise the impact of subsurface volume scatter. As a consequence, threshold retrackers tend to exhibit lower elevation residuals in analyses of single-cycle cross-overs [*Davis*, 1997; *Helm et al.*, 2014], which suggests improved repeatability of elevation measurements, with respect to varying antenna orientation and errors which decorrelate over the orbit cycle (Figure 6). This superior repeatability has been used as an argument for using a threshold retracker to measure rates of ice sheet elevation change [*Davis*, 1997; *Helm et al.*, 2014], on the basis that it offers improved stability over time. However, this argument assumes that stability with respect to antenna orientation implies stability with respect to time. Given what is currently known about the different characteristics of the surface and subsurface echo, it remains unclear whether such an argument holds. Previous analysis [*Arthern et al.*, 2001] of deconvolved LRM waveforms in the interior of the Antarctic Ice Sheet, for example, suggested that although volume scatter can be highly anisotropic, as a consequence of anisotropy in the extinction coefficient resulting from scattering out of the beam, it is more stable in time in comparison to the surface reflection. This may imply that although a surface-orientated retracker minimises cross-over residuals, a retracker which also utilises the volume echo might be better suited to studies of elevation change. However, it may also be the case that retracking based upon a power threshold on the first leading edge avoids some of the difficulties of multi-peaked waveforms in regions of complex topography (Figure 5). This example illustrates the challenges associated with assessing retracker performance and why, at present, there is no clear consensus on what method of retracking is optimal for studying ice sheet elevation change.

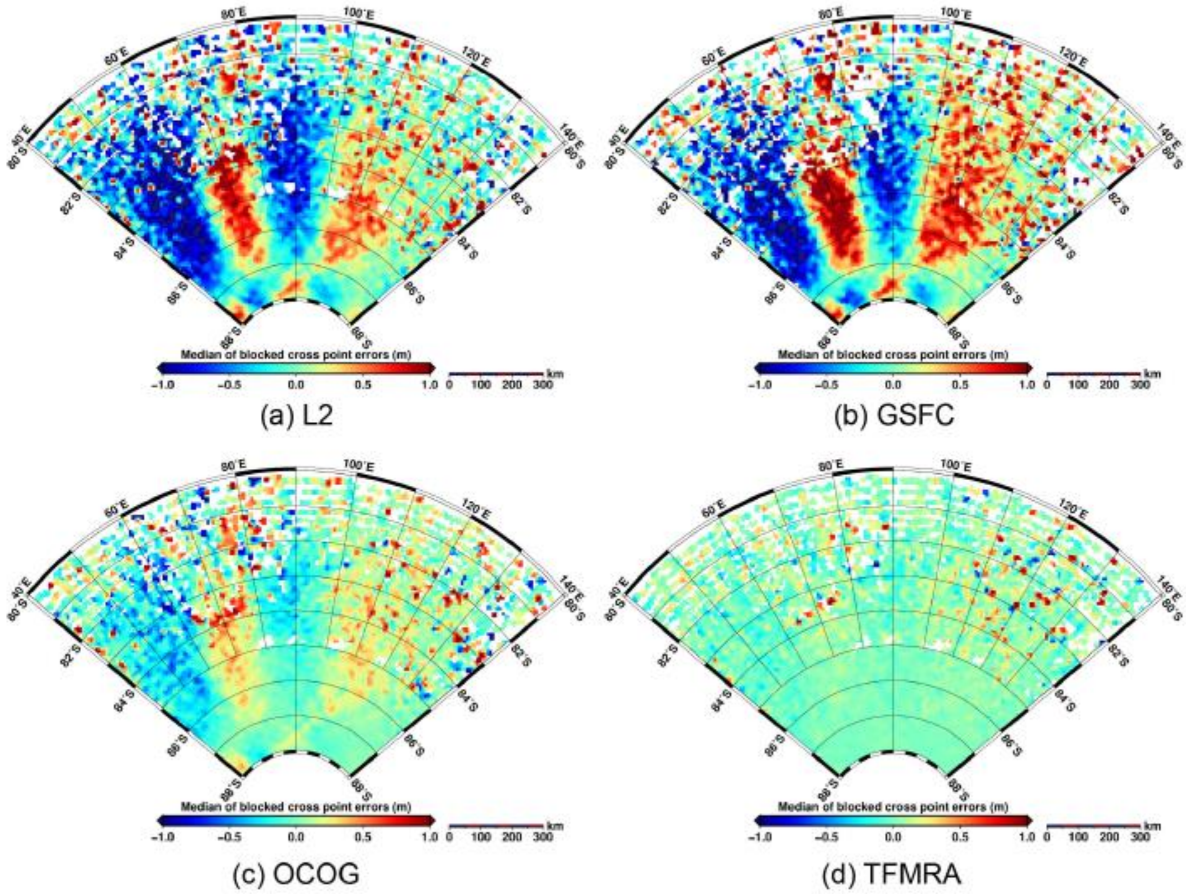

Figure 6. LRM median single-cycle cross-over elevation residuals retrieved over central Antarctica using (a) ESA CFI retracker, (b) NASA β-parameter retracker, (c) OCOG retracker and (d) threshold retracker, from *Helm et al.* [2014].

3.3.2. Slope Correction Methods

When radar altimeters acquire data over the sloping topography of ice sheets, consideration must be given to the displacement of the echoing point from nadir. In general, the strongest power return within the beam footprint will come from locations where the surface is orthogonal to the direction of the incident radar wave. Over a broadly flat surface, such as the ocean, this point is located at nadir. However, for a more irregular surface such as an ice sheet, the point of orthogonality, which in the case of a uniform slope across the beam footprint is co-located with the point of closest approach, will be off-nadir and up-slope (Figure 7). In this case, the echoing position is offset laterally in proportion to the magnitude of the slope, and in the direction of maximum gradient. Depending on the gradient of the slope, the lateral relocation can be of the order of kilometres and the corresponding vertical adjustment can be tens of meters.

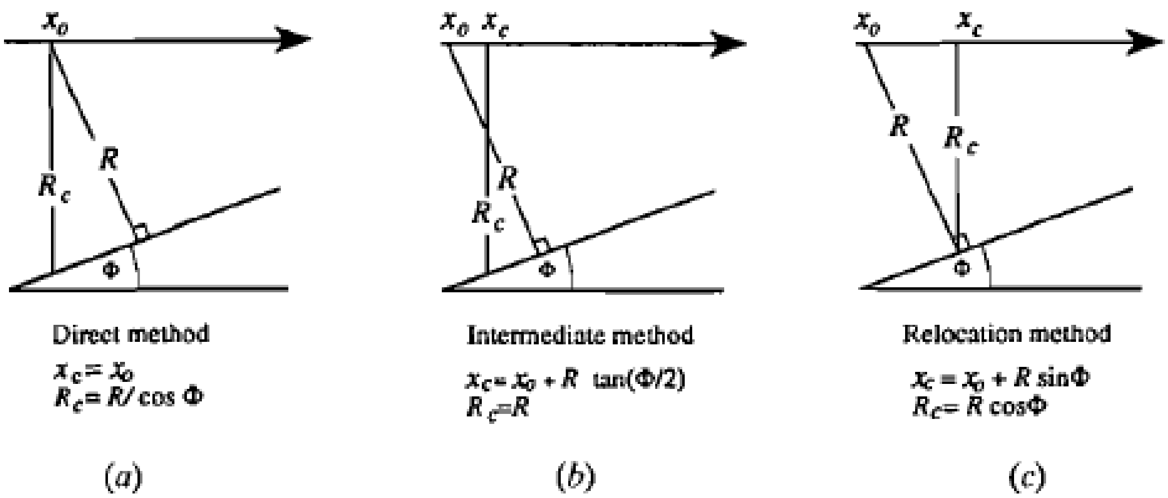

Figure 7. Illustration in 2-d of the different methods used for the slope correction of radar echoes, where x_0 and R are the initial satellite position and range respectively, x_c and R_c are the corrected location and range respectively, and ϕ is the angle of surface slope, from *Bamber* [1994].

Although it may be argued for studies of elevation change that the time invariant influence of slope will cancel in the differential height, it will nonetheless lead to a location error in the positioning of the measurement. This in turn can introduce biases into the interpretation of these data [*Hurkmans et al.*, 2012]. Therefore, in conventional, non-interferometric radar altimetry, a slope correction based on external data is usually applied [*Brenner et al.*, 1983; *Remy et al.*, 1989; *Bamber*, 1994]. This correction accounts for the fact that the true point of reflection is not at nadir. Three methods are commonly used for this slope correction (Figure 7), the direct method [*Brenner et al.*, 1983], the intermediate method [*Remy et al.*, 1989] and the relocation method [*Bamber*, 1994]. The direct method adjusts the range at nadir, the relocation method adjusts the measurement position to its estimated true position at the point of closest approach, whilst the intermediate method adjusts the location such that the measured range to surface is maintained. These methods are illustrated schematically in Figure 7. Of these, the relocation method aims to place the height measurement at the actual point where the pulse-limited footprint is centred (Figure 7c), therefore representing the true echoing location. For most applications, particularly over more steeply sloping terrain, this approach may be considered preferable, as it avoids attributing measurements to inaccurate locations which can lead to inappropriate geophysical interpretation [*Hurkmans et al.*, 2012]. Since these original concepts of slope correction were introduced, further refinements to these methods have been made [*Roemer et al.*, 2007], for example by making direct use of an external Digital Elevation Model to identify the point of closest approach and to compute the associated slope correction (Figure 8).

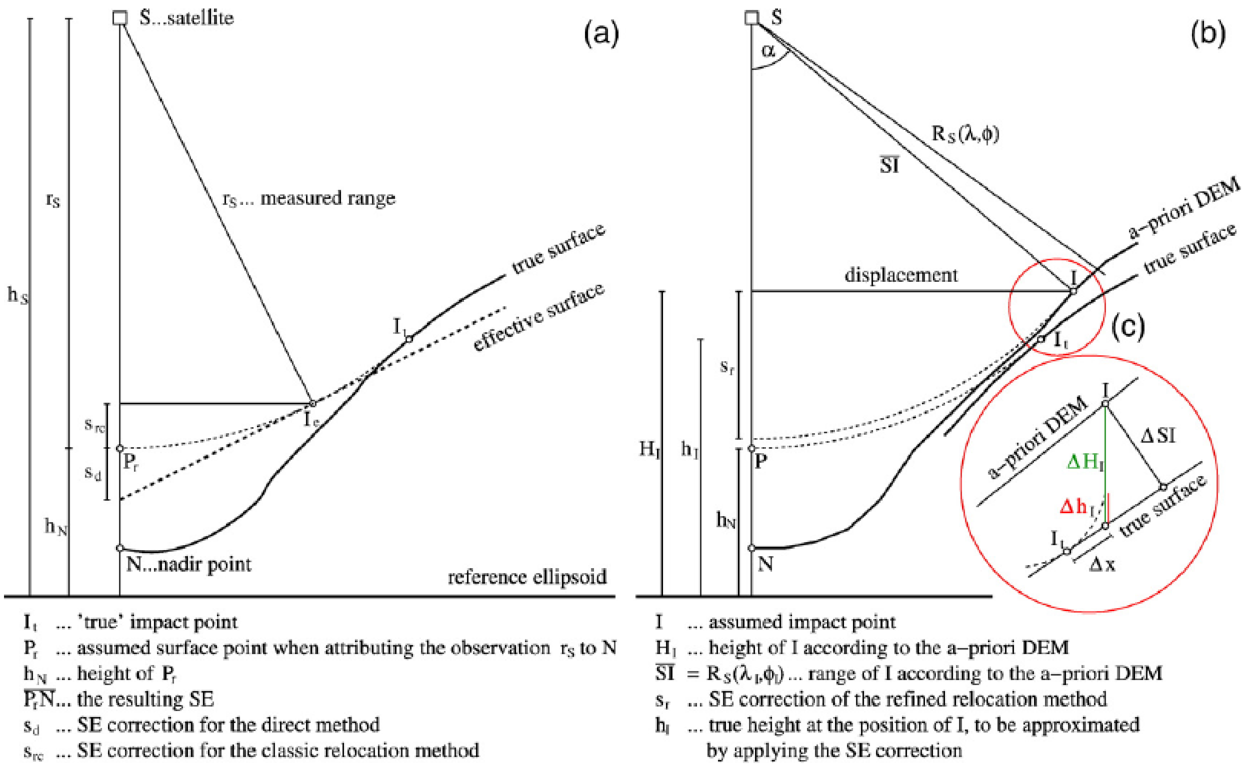

Figure 8. Geometry of slope correction for the direct and classic relocation methods (a) and for a refined approach which utilises surface elevations from a Digital Elevation Model (b), from *Roemer et al.* [2007].

The use of the relocation method for slope correction has the effect of producing less homogenous sampling, as measurements tend to cluster on topographic highs and be absent from depressions. However, as clearly shown from interferometric SAR altimeter measurements, this is a reflection of the true performance of the radar system, with its tendency to sample elevated regions, and so in itself should not act as a reason to favour an alternative method.

3.4. Determination of Ice Sheet Elevation Change

One of primary applications of radar altimeter measurements over ice sheets is that of estimating surface elevation change from repeated measurements of ice sheet surface elevation. These observations are central to many studies of ice sheet mass balance and sea level contribution and therefore within any assessment of altimeter processing it is important that not only elevation, but also elevation change, be considered. In this section we therefore review the two principle methods that are used this purpose, which are commonly referred to as the cross-over [*Wingham et al.*, 1998; *Zwally et al.*, 2005] and repeat-track [*Pritchard et al.*, 2009; *Flament and Rémy*, 2012; *McMillan et al.*, 2014] techniques. We note that alternative approaches do exist [*Moholdt et al.*, 2010], although these are much less common and are therefore not discussed in detail here. We conclude this section with an overview of the relative advantages and disadvantage of each of these principle techniques.

3.4.1. Cross-over Technique

The first technique developed for analysing ice sheet elevation change from repeated elevation measurements was the cross-over technique [*Wingham et al.*, 1998; *Zwally et al.*, 2005]. This method has now been in use for twenty years and the algorithms are well-established within the scientific literature [*Davis et al.*, 2005; *Zwally et al.*, 2005; *Khvorostovsky*, 2012; *Shepherd et al.*, 2012]. Here we provide a brief overview of the approach. This method computes elevation differences at the intersection of two satellite ground-tracks, one ascending and one descending (Figure 9). In practice, altimeters deliver discrete measurements, usually sampled every ~340 m along the ground track, and so interpolation of bracketing elevation records is required to determine heights at exact cross-over locations.

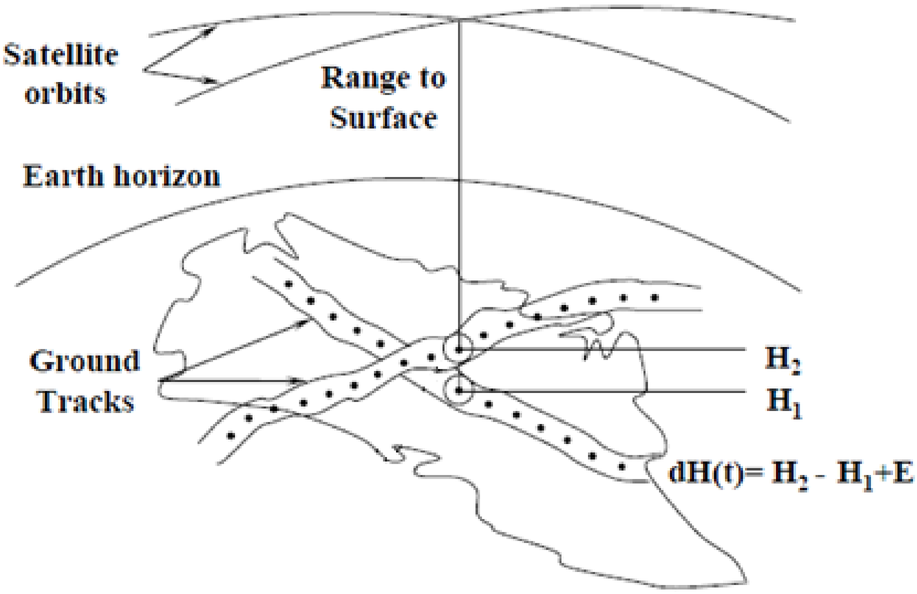

Figure 9. Illustration of the cross-over technique, from *Davis* [1995].

The measured elevation difference at a crossover point has contributions from both the detected surface elevation difference and errors due to measurement and orbital imprecision. The surface elevation difference will include both temporal change and differences due to the differing orientation of the antenna, for example due to the interaction of a linearly polarised radar wave with a non-isotropic snowpack.

When crossing two cycles of data there are two potential crossovers at each intersection, one where the ascending track is taken from the first cycle and one where the descending track is taken from the first cycle. Therefore the elevation difference between any two cycles at any crossover location is usually calculated as the average of the two crossover calculations, with the average elevation difference when the same cycle is crossed used to estimate the uncertainty associated with each relative height measurement [*Wingham et al.*, 1998].

By designating one cycle as a reference cycle, and then repeatedly crossing it with a succession of orbit cycles, a time-series of height differences can be generated. Alternatively, multiple reference cycles can be introduced, in order to maximise data coverage. Commonly elevation differences from all cross-overs within a specified search region are averaged in order to supress noise. Most methods also apply an empirical backscatter correction to account for the covariance between changes in backscatter and elevation [*Wingham et al.*, 1998; *Davis et al.*, 2004]. To derive rates of elevation change, a model is then fitted to the data (Figure 10). Various different functional forms have been used for this purpose, but most commonly either a linear plus sinusoidal function is used to account for secular and seasonal cycles [*Wingham et al.*, 1998; *Shepherd et al.*, 2012] or an auto-regressive model [*Davis et al.*, 2004] is used. Cross-over density varies as a function of latitude, with the highest density found close to the latitudinal limit of the satellite orbit and decreasing towards the equator. As a result of this and the typically monthly repeat cycle, cross-overs do not tend to offer complete coverage of the ice sheets. In Antarctica, for example, peripheral regions tend to be more sparsely sampled. This is further exacerbated by lower coverage due to the altimeter losing lock in areas of more complex terrain, and means that a certain degree of interpolation is required to achieve comprehensive coverage.

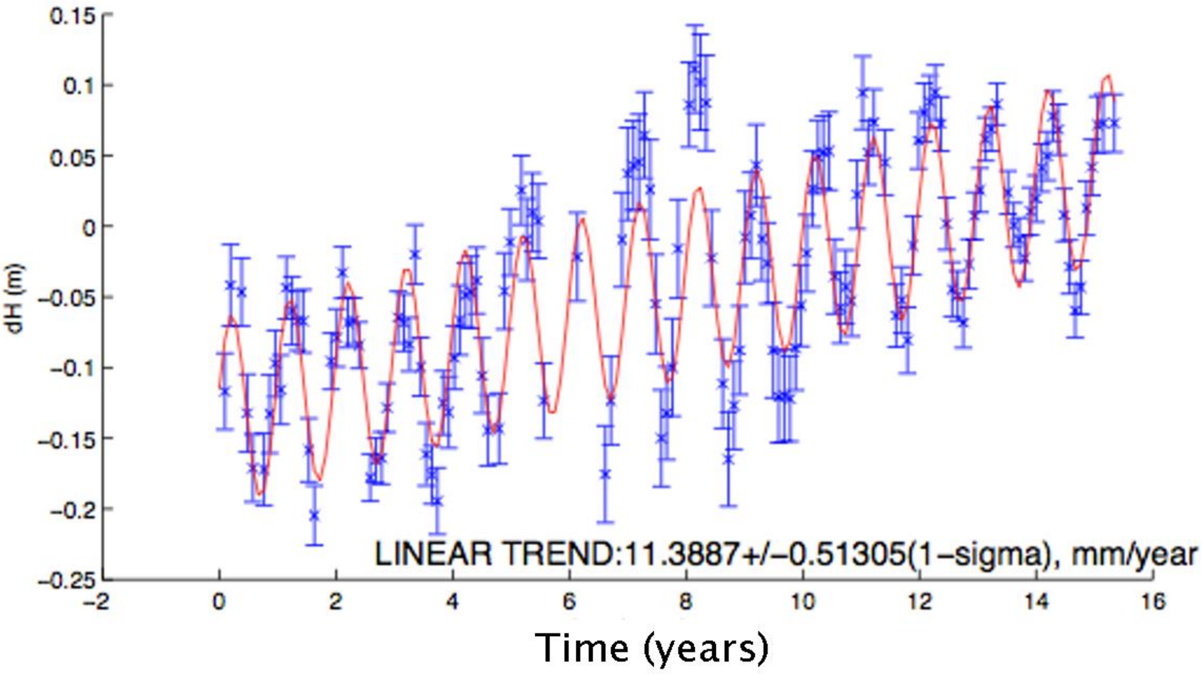

Figure 10. Example of deriving an elevation rate estimate using relative height measurements derived using a cross-over technique. Here a linear plus sinusoidal function has been fitted to the relative height measurements.

3.4.2. Repeat-track Technique

The repeat-track approach, also known as the along-track or model-fit method, extends elevation retrieval beyond the locations of orbit cross-overs to include all data acquired along the satellite track [*Pritchard et al.*, 2009; *Smith et al.*, 2009; *Moholdt et al.*, 2010; *Flament and Rémy*, 2012; *McMillan et al.*, 2014]. Data acquired over a succession of orbit cycles are grouped according to spatial proximity, either by dividing a defined reference track into segments or by considering near-repeats from adjacent tracks. Data within each segment are distributed in space, both along-track with successive measurements and across-track because of satellite drift within the orbit dead band, and also in time, with acquisitions over a succession of orbit cycles. This dispersion in space and time can be used to simultaneously solve for the spatial (i.e. topography) and temporal (i.e. rate of change) contributions to the elevation fluctuations apparent within each segment (Figure 11). In practice, this approach, like the cross-over technique, requires a model to be fitted to the data. In the case of the along-track method, the model must also include spatial, as well as temporal dimensions. Topography is usually modelled as a first [*Smith et al.*, 2009; *Moholdt et al.*, 2010] or second [*Flament and Rémy*, 2012; *McMillan et al.*, 2014] order polynomial, depending upon the neighbourhood size over which measurements are grouped. The model can also be extended to account for additional influences on the elevations fluctuations, such as elevation offsets between ascending and descending tracks caused by anisotropic volume scattering [*McMillan et al.*, 2014] or other waveform parameters [*Flament and Rémy*, 2012]. As with the cross-over technique, it is common for a backscatter correction [*McMillan et al.*, 2014], or indeed corrections based upon multiple waveform parameters [*Flament and Rémy*, 2012], to be implemented.

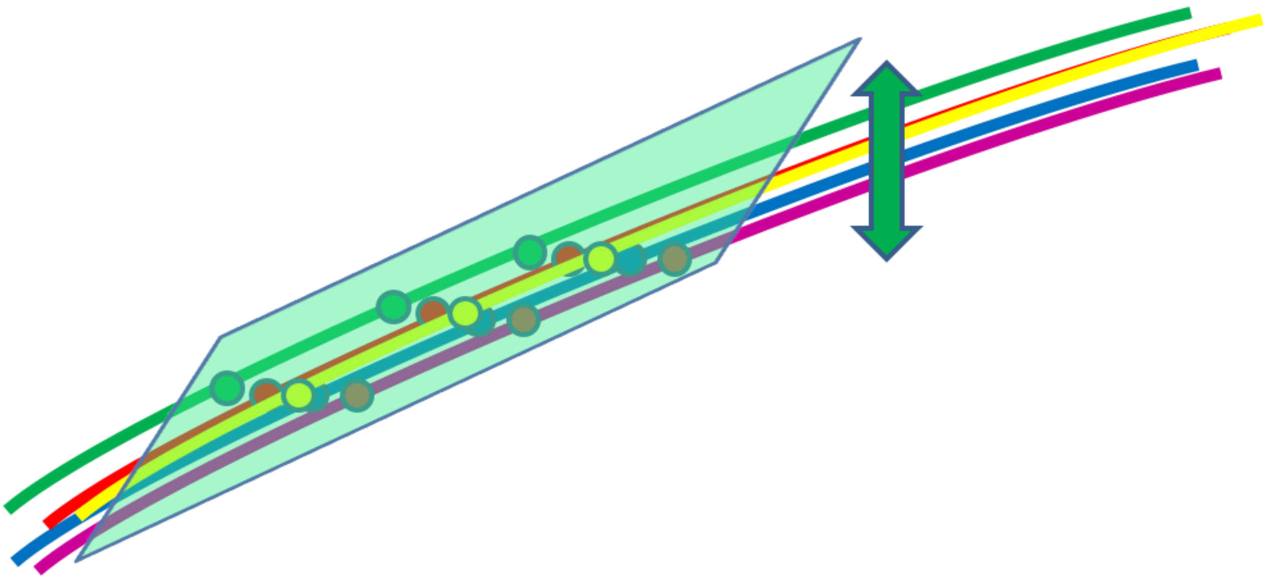

Figure 11. Illustration of the repeat track method whereby a plane, which is allowed to migrate in the vertical axis as a function of time, is fitted to the elevation measurements within a track segment.

3.4.3. Comparison of Cross-over and Repeat-track Techniques

Cross-over and repeat-track techniques each have their own distinct advantages and so the choice of method will be influenced by the specific dataset and scientific application. Here we briefly summarise the principles benefits of each technique. Early on, the cross-over approach was used in most analyses of ice sheet elevation change [*Wingham et al.*, 1998; *Davis et al.*, 2005]. However, in more recent years, repeat-track techniques have become more popular [*Pritchard et al.*, 2009; *Flament and Rémy*, 2012; *McMillan et al.*, 2014]. The principle advantage of the cross-over methodology is that elevation differences are computed at the intersection of tracks, and so direct slope induced errors are less severe. Indirect slope effects can still, however, degrade these measurements and must be taken into account during data analysis [*Hurkmans et al.*, 2012]. The main advantage of the repeat-track method is the increase in data volume and coverage. This arises because data acquired along the entire satellite track can be utilised and also because elevation rates can be derived from data acquired from a single pass direction, therefore avoiding some of the problems associated with the altimeter losing lock as it passes from ocean over the coast [*Flament and Rémy*, 2012]. As a result, repeat-track techniques achieve much more comprehensive sampling than cross-over techniques, which implies a lesser need for data interpolation techniques and reduced risk of biased estimates, for example caused by under-sampling regions of the ice margin where the magnitude of changes is greatest. Repeat-track techniques are particularly well-suited to satellites with a long orbital period, such as CryoSat-2, where individual cross-over points are only sampled relatively infrequently.

3.5. Studies of Radar Wave Interaction with the Snowpack

The radar wave interaction with the snowpack has always been subject to interrogation considering the penetration depth in Ku band which depends a lot on the physical properties of the surface (structure, temperature, etc). The penetration depth is theoretically reduced from around 10 m in Ku-band, to less than 1 m in Ka-band, such that the volume echo originates from the surface or the near subsurface. The SARAL/AltiKa mission (Indian Space & Research Organization (ISRO) and CNES cooperation mission launched in February 2013), gives us the first opportunity to compare Ku band and Ka band measurements (AltiKa is a single frequency altimeter in Ka band - 36 GHz - flying along the historical Envisat ground track). It also offers a unique opportunity to better characterize the Ku-band radar penetration depth into the snowpack with respect to the Ka one and consequently to better quantify the potential errors that could affect the historical altimetry dataset.

Moreover, the sharper antenna pattern in Ka band (0.6 degrees) leads to a fast decreasing trailing edge that reduces the impact of the ratio between surface and volume echoes of the height retrieval. Indeed, the spatial and temporal observations of AltiKa at cross-over points and along-track, indicate that the impact of backscatter changes on the height decreases from 0.3 m/dB for the Ku-band to only 0.05 m/dB for the Ka-band. Therefore, the height measurement is really very stable over time. Moreover, the volume echo, in Ka-band, results from the near subsurface layer and is mostly controlled by ice grain size, unlike the Ku-band. As a consequence, the Ka measurement can be considered as a very good reference for analyzing Ku band echoes which can be those obtained by Cryosat-2 in the conventional LRM mode but also those obtained in the new Delay-Doppler mode that will be operational everywhere on Sentinel-3.

During the Constanz OSTST (2014), a first Ku/Ka band comparison has been presented at crossovers over very flat surfaces in Antarctica (Vostok lake). An illustration of the individual echoes over these surfaces is presented in Figure 12, showing a very good consistency between all waveforms of the segment (in Ku and Ka bands). All waveforms have been corrected for the aperture at -3dB of the antenna gain pattern which is largely different in Ku and Ka bands (around 1.15° for CryoSat-2 and 0.605° for SARAL). The location for this comparison has been chosen in order to remove any surface slope effects (close to 0 in this case). The difference of penetration depth that can be observed on the width and inclination of the two leading edges. For each graph, the blue plots represent the mean uncorrected waveform.

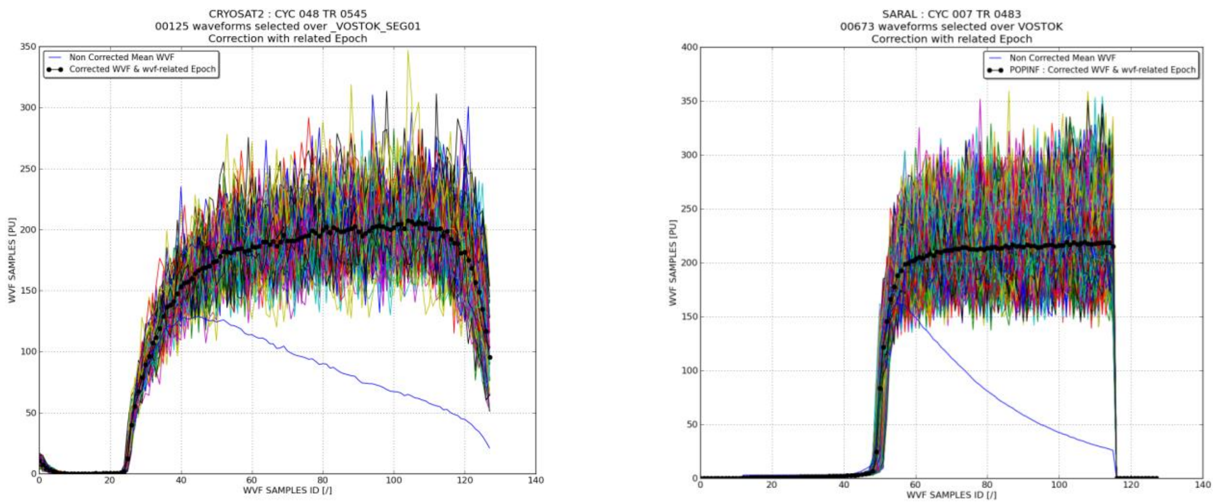

Figure 12. CryoSat-2 (on the left) and Saral (on the right) individual corrected waveforms over the Vostok lake (CryosSat-2 - track 545; SARAL - track 483).

As well, Figure 13 illustrates the same differences between Ku and Ka band waveforms but on the mean CryoSat-2 and SARAL waveforms over the Vostok lake.

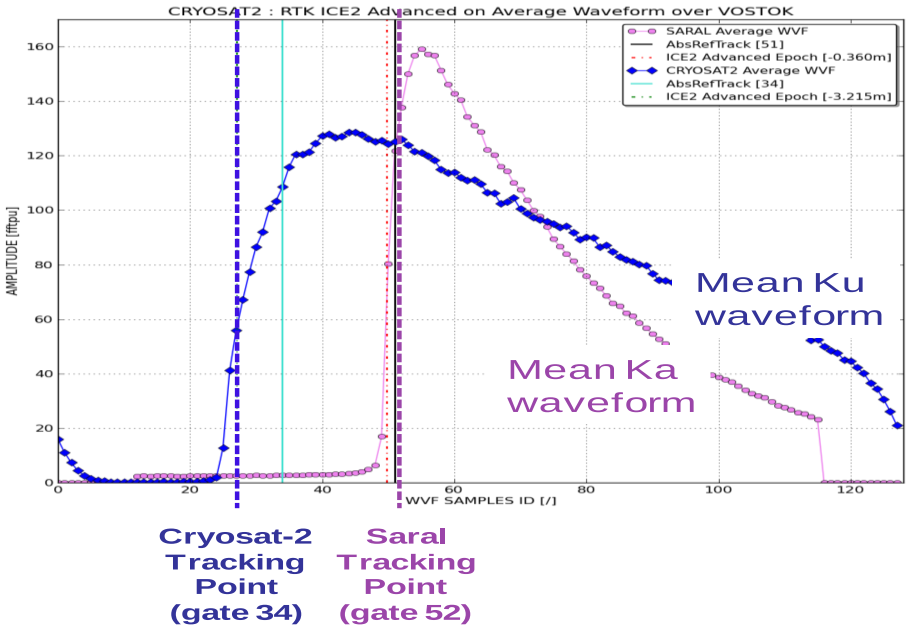

Figure 13. Collocated Ka (AltiKa in purple) and Ku (Cryosat-2 in LRM in blue) mean measurements over the Vostok lake in Antarctica.

These comparisons have been obtained considering CryoSat-2 operating in LRM mode. Similar analyses must be conducted with RDSAR and with SAR waveforms. We can anticipate that SAR waveforms will be much less impacted by the volume echo than in LRM/RDSAR modes and that the leading edge of the echo will not be affected as in LRM/RDSAR modes. Again, because the antenna pattern is very narrow in Ka band, it is crucial to perform this comparison over very well known flat surfaces in order to avoid slope terrain effects on the waveforms and misinterpretation of the acquired signals.

Comparison between Ku and Ka waveforms should help to better understand the radar wave interaction with the snowpack. However, this comparison should not be complete without an in depth comparison of the geophysical parameters computed by the retracker algorithm. As explained in the previous chapters, the choice of the retracker is thus crucial to compare the geophysical estimates computed from these two waveform shapes. Analyzing/monitoring the snowpack changes using measurements from a unique mission may simply make use of simplified models of the radar returns and/or simplified methods (retracker). The reason is that approximations (instrumental for example) can be considered to be constant over time.

However, when processing/comparing measurements from different missions, approximations can introduce differences interpreted as geophysical differences. So we must be very careful on methods that are used to derive geophysical parameters.

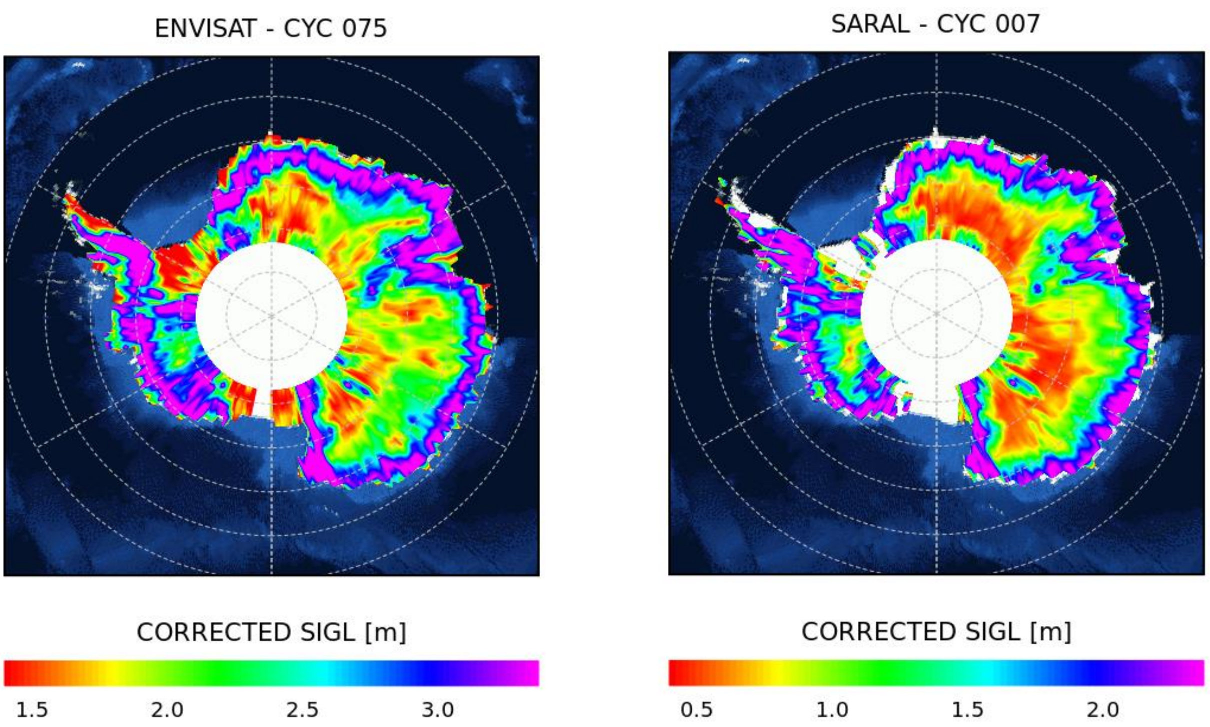

Figure 14. Ku (Envisat/RA-2) and Ka (Saral/AltiKa) leading edge widths over Antarctica.

At Cryosat-2 crossovers, an analysis can be conducted in order to analyze the surface anisotropy. The volume echo affects the elevation and backscatter differences at cross-over points. The impact depends on the angle between the antenna polarization direction and the prevailing roughness direction. This difference is due to the volume echo, the anisotropic characters of the surface and the angle between the descending and ascending tracks [*Remy et al.*, 2012]. This effect is usually assumed to be stationary, but obviously the volume echo may vary with time. This could be a limitation when estimating the volume balance. Note that the absence of this effect at some cross-overs does not imply the absence of a volume echo. Instead, this observation may be due to the absence of surface anisotropy or to a particular orbit configuration.

With the help of two frequencies, for instance, using a dual-frequency altimeter (such as Ku- and S-band sensors onboard Envisat) or different altimeters (Figure 14) in the same orbit (e.g., Envisat and AltiKa), a direct comparison between height and backscatter differences may permit the detection of the volume echo and estimation of the impact on height retrieval.

3.6. Existing Challenges for Conventional Altimetry

Over ice sheets, the principle challenges associated with conventional altimetry relate to the size of the ground footprint and the complex nature in which the radar wave interacts with a spatially and temporally variable snowpack. In the case of the former, locating the echoing point within the beam footprint can be challenging, and complex topography can distort the waveform shape and affect retracker performance. In the case of the latter, understanding the complex nature of these effects on the waveform shape can be difficult and as a result can produce greater uncertainty in altimeter estimates of elevation and elevation change.

In regions of complex and irregular terrain, tracking may also fail, as the predictive capability of the commonly-used closed-loop tracking may not be able to adequately resolve the true topographic variability. This can lead to significant data loss, which often tends to be focussed on the regions which are changing the most rapidly, such as narrow outlet glaciers surrounded by high peaks. Here altimeters may benefit from new trackers that use high quality pre-existing information to position the analysis window.

4. SAR Altimetry

4.1. The Development of SAR Altimetry

In this section we provide a brief overview of the past, present and future developments in SAR altimetry. Synthetic Aperture Radar (SAR), or Delay-Doppler, altimetry was first implemented on a NASA mission to Venus [*Ford and Pettengill*, 1992]. Subsequently, airborne SAR systems were developed and demonstrated for Earth Observation purposes [*Raney*, 1998], and used to support the development of ESA's CryoSat satellite [*Wingham et al.*, 2006]. The first Delay-Doppler Processor used with altimeter data from a European Earth Observation satellite was a Ground Processor Prototype (GPP) developed by UCL for the CryoSat-2 mission. This GPP was used for validating CryoSat-2 products and the end-to-end processor chain performance. This GPP was later operationally adapted by Aresys to become the SAR and SARin chains of the Instrument Processing Facility 1 of the CryoSat-2 mission.

In CryoSat-2, new, intermediate, lower-level products such as Full Bit Rate (FBR) and calibrated FBR (C-FBR) products, equivalent to the so called L1A products in Sentinel-3 and Sentinel-6, were originated with the main purpose of testing, debugging and internally verifying the processor algorithms. In addition to that, some calibration and validation activities also needed customised L1 algorithms that were different to the baseline ones provided in the L1B GPP.

Building upon these past experiences, the Sentinel-3 mission inherited all the lessons learnt by the CryoSat-2 and Jason-2 missions, and a new L0/L1 Delay Doppler Ground Processor Prototype (GPP) was defined and implemented. This GPP was developed, tested and validated by isardSAT, based on the algorithms defined by CLS (see Surface Topography Mission – L0 and L1b SRAL Algorithms Definition, Accuracy and Specification, S3-RS-CLS-SY-00017, issue:10.0, 3 April 2013). This definition, together with the lessons learned from the GPP implementation, was later used to implement the Sentinel-3 Instrument Processing Facility by ACRI ST and CLS companies (see Sentinel-3 Core Payload Data Ground Segment (PDGS) Instrument Processing Facility (IPF) Implementation-Detail processing Model-SRAL Level 1, S3IPF.DPM.005, Issue: 2.1, 11 February 2014).

In 2013, ESA released L1 and L2 processor prototypes called SARvatore: SAR Versatile Altimetric Toolkit for Ocean Research & Exploitation (GPOD CryoSat-2 SARvatore Software Prototype, on-line user manual). This processor offered to the scientific user community the capability for ocean-dedicated L1 Delay-Doppler processing, and also the opportunity to produce customised L1 Delay-Doppler products from L1A products (CryoSat-2 FBR products). These processing capabilities include the application of Hamming weighting window and the selection of the size of the radar receiving window.

Looking to the future, and with a view to upcoming missions, new developments in Delay-Doppler processing are currently being implemented. These are in preparation for Sentinel-6/Jason-CS, which will be the continuity of previous conventional altimetry Jason's missions but with a new SAR altimeter (Poseidon-4) on-board. The main differences between the Sentinel-3 altimeter (SRAL) and the Sentinel-6 altimeter (Poseidon-4) are:

1. Improved digital and radio frequency hardware.
2. Open burst Ku-band pulse transmission (interleaved mode). This mode performs a near continuous transmission of Ku-band pulses. It will allow simultaneous processing of the measurements to obtain High Resolution along-track (HR or SAR) and Low Resolution along-track (LR or LRM) data.
3. As with previous satellite radar altimeters, the Poseidon-4 transmits C-band pulses in order to retrieve a correction for ionospheric path delay. However, permanent calibration pulses will also be integrated within the transmission pattern without the need to switch between working modes.

4. Implementation of on-board “Range Migration Correction” (RMC) processing in order to reduce the amount of data that must be downlinked.

The Ground Prototype Processor of the Sentinel-6 mission altimeter, Poseidon-4, is being developed by isardSAT under an ESTEC/ESA contract that started in 2011 and which lasts until the end of the satellite Commissioning phase. This processor includes new features partly thanks to the experience gained with the CryoSat-2 data and partly thanks to the many studies carried out during the development of the project. This development has taken advantage of simulated data produced by the ESTEC Sentinel-6/Jason-CS mission performance simulator. This simulated data has proven to be extremely useful for the understanding of the details of Delay-Doppler Processing, which is still relatively new in the altimetry world. The fact that a new configuration had to be addressed has also invited the review of some of the theory, coming up with new methodologies in different aspects of the processing.

4.2. Overview of SAR Processing Concept

This section outlines the principle steps of the SAR, or Delay-Doppler, processing concept. Figure 15 shows the generic L1A/L1B SAR processing chain algorithms and output products. Each process is addressed in turn below.

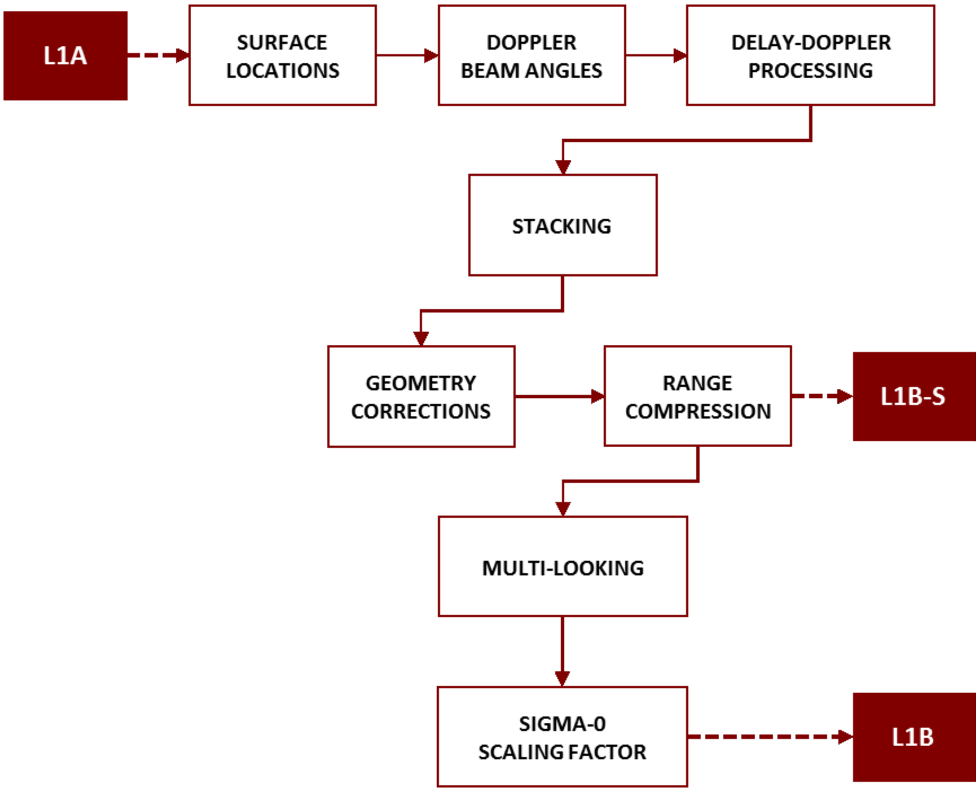

Figure 15. Level-1 SAR-Ku chain.

Determine surface type

This algorithm computes the surface type ("open ocean or semi-enclosed seas", "enclosed seas or lakes", "continental ice" or "land") determining the point of a "land-sea mask" Auxiliary Data File nearest to the geolocated measurement. The latitude and longitude resolution of this land-sea mask is 2 minutes.

Surface locations

The L1B results are based on the surface sampling that has been performed. This algorithm is responsible for computing the spacing between the surface locations, considering the satellite Doppler resolution and the surface profile. This prevents the surface from being oversampled or gaps being left.

The first step in computing the surface locations is to build an estimated surface. This is done using the satellite burst positions and the window delay (also called the tracker range). Then the first surface location is initialised with the values of the first burst. After that, an iterative process starts to compute the rest of the sampling, which is repeated until the end of the orbit data is reached (see Figure 16). The steps involved are:

- Compute the angular Doppler resolution, α, through the Doppler frequency expression.
- Determine the intersection of this direction with the surface. This process is performed by iterating through the surface positions until the angle of sight is bigger than the angular Doppler resolution (see Figure 16).
- Once this is done, an interpolation of the surface is performed between the two last surface positions. In CryoSat-2, this is done with a linear interpolation. On the other hand, in Sentinel-3 this interpolation is done with cubic splines. With this, a new surface location and its datation is found.
- After that, all the orbit parameters (satellite equivalent position, satellite velocity vector, satellite attitude) are computed with the new datation. Again, these parameters are obtained by use of an interpolation (linear in CryoSat-2 and splines in Sentinel-3).

Then, the process starts again, taking as a reference this last surface location and its corresponding orbit parameters.

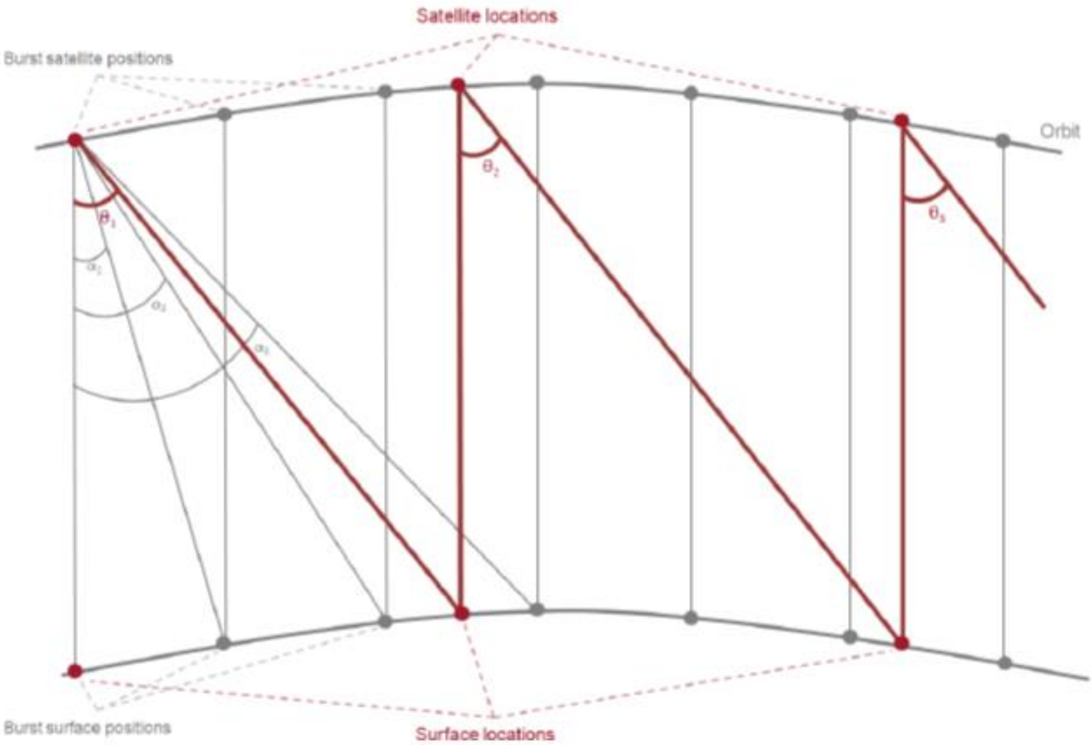

Figure 16. Computation of surface locations (Credit: isardSAT).

Doppler beam angles

In order to be able to perform the Delay-Doppler processing, the angles between each satellite burst position and all the surface locations that have been illuminated have to be computed. This algorithm that determines these directions and its geometry is shown in Figure 17. Note that the Doppler spectrum is divided into 64 bins since each one is then associated to each pulse, that with the azimuth processing, will be converted into a Doppler beam.

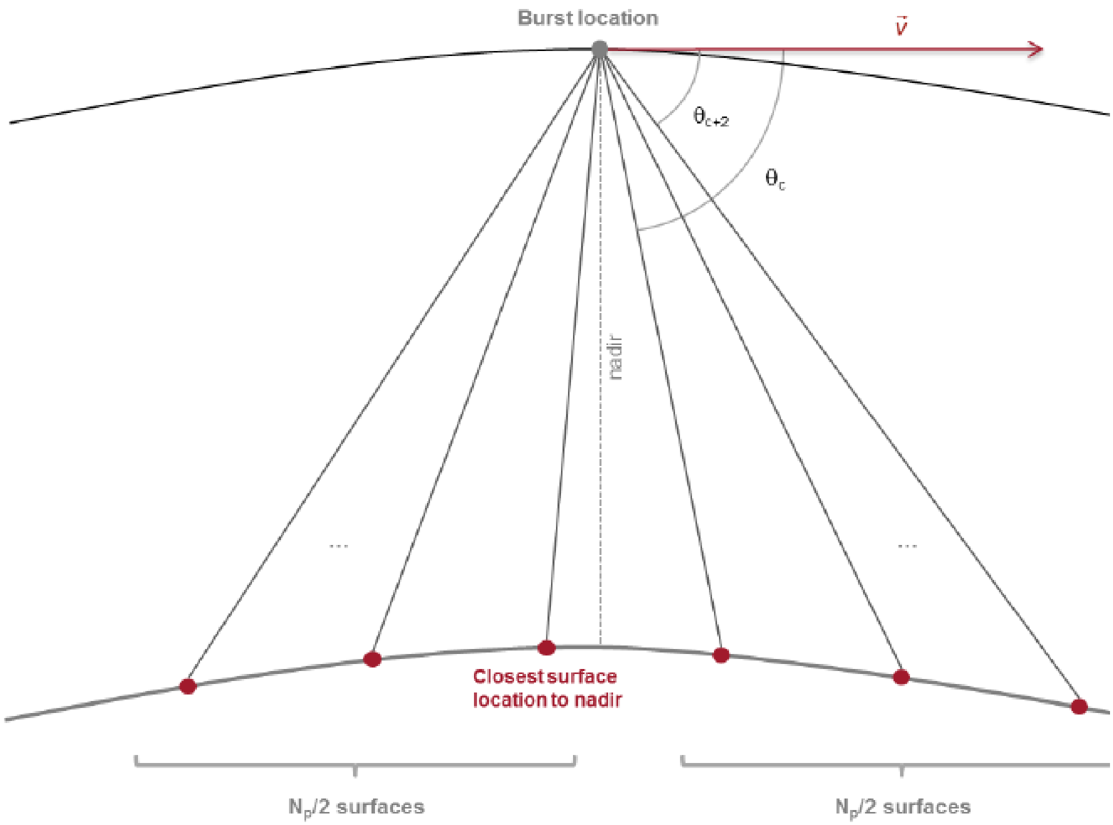

Figure 17. Determine Doppler beams direction (Credit: isardSAT).

Delay-Doppler Processing

This algorithm creates the Delay-Doppler beams, each one steered to a different surface location. This is done by applying an FFT in the azimuth direction to all the pulses within a burst, which allows the conventional altimeter footprint to be divided into a certain number of strips and thus the creation of the Delay-Doppler Map (DDM).

There are two ways of building the DDM: with a constant ground spacing, used only for low variability surfaces, or with a more precise method, with variable ground spacing, that can be used for all kinds of surfaces (although it requires more computational time since it applies one FFT for each Doppler beam instead of one for the entire burst).

Stacking

From the DDM, all contributions coming from different strips can be identified and collected separately. When all the contributions from different bursts are collected, a stack is formed. Thus this process is called stacking (Figure 18).

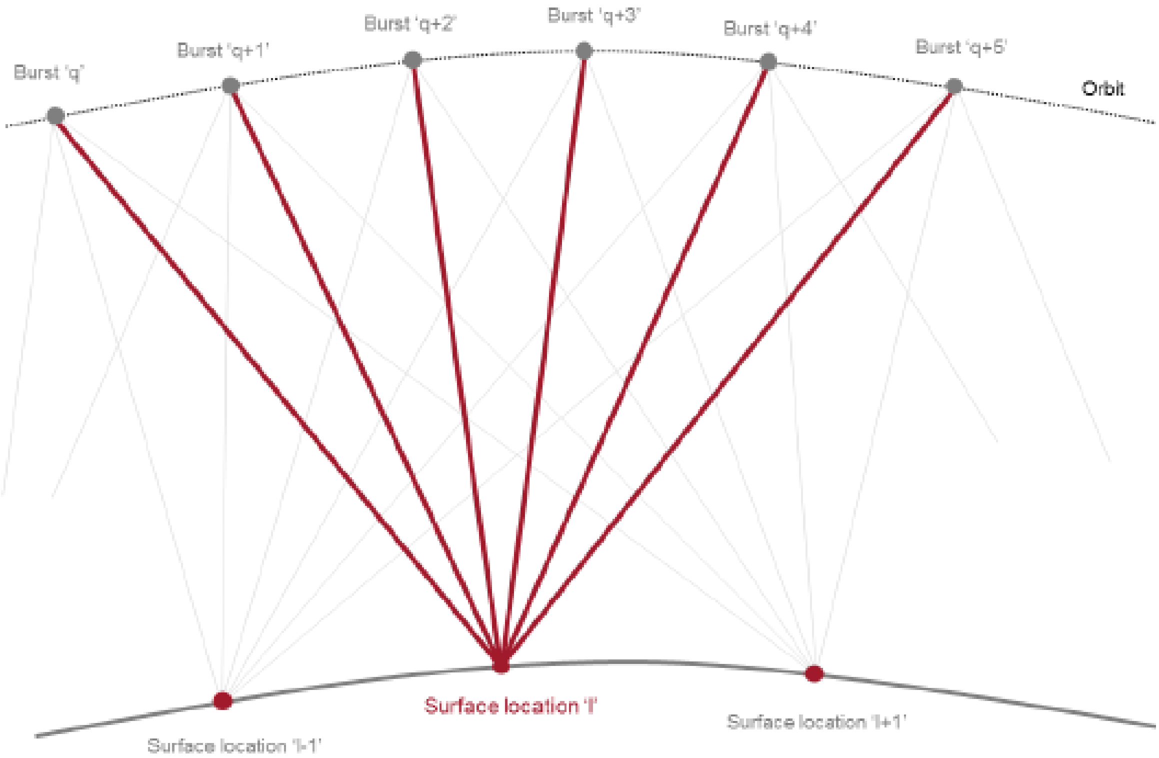

Figure 18. Stacking process for surface location 'i'.

Geometry corrections

This algorithm computes and applies all the corrections associated with the geometry. These are the Doppler, slant range and window delay misalignments corrections.

- *Doppler correction*. Due to the movement of the satellite with respect to the surface, Doppler frequencies are generated for each Doppler beam. Hence, a compensation to this phenomena has to be applied. This is depicted in Figure 19.

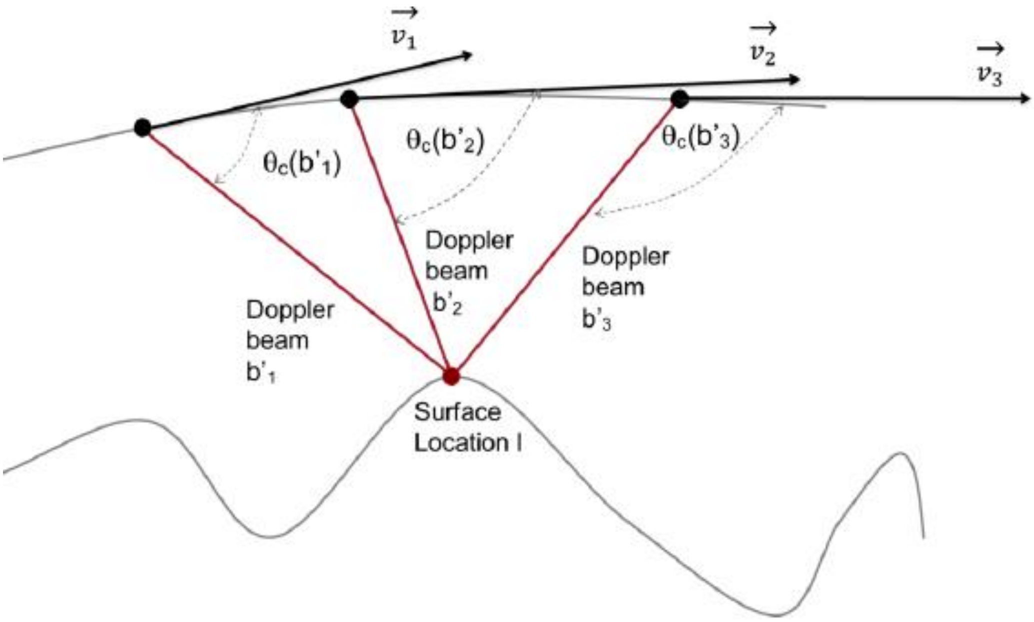

Figure 19: Doppler shift effect (Credit: isardSAT).

- *Slant range correction*. Off-nadir beams suffer a range migration effect. This means that these beams have different (and greater) round-trip distances than the nadir beam and so a compensation must be applied. The geometry of this scenario is shown in Figure 20.

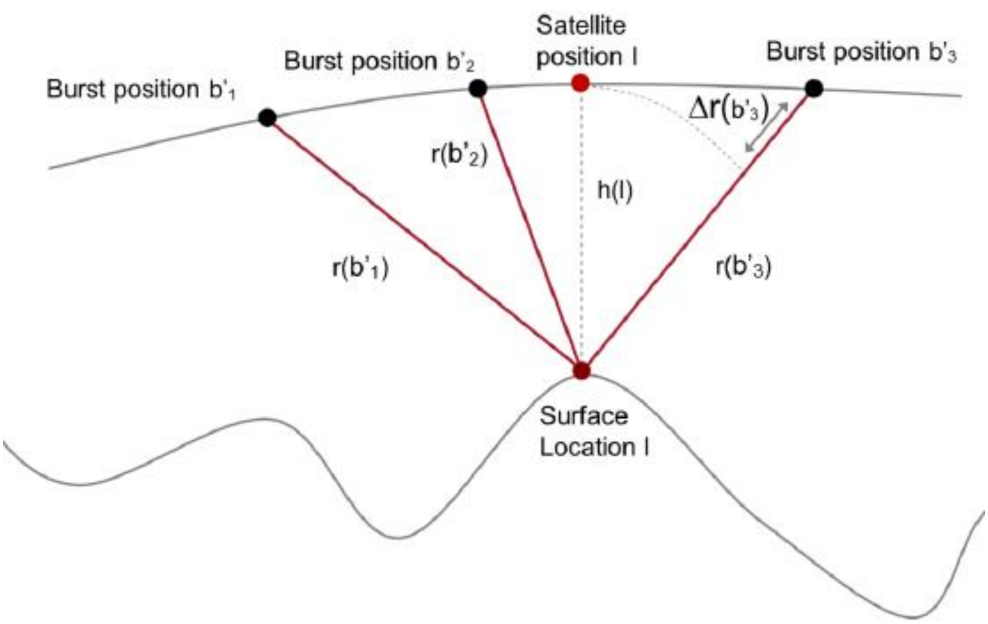

Figure 20. Slant range correction (Credit: isardSAT).

- *Window delay misalignments*. Since all the beams that form a stack come from different bursts, they were received with different window delays. This results in a misalignment of the different beams and has to be corrected.

All these geometry-based effects are observed as a range misplacement within the receiving window. This can be seen when showing a plot of a range-compressed stack. Once the corrections have been compensated, the stack is then range aligned (Figure 21).

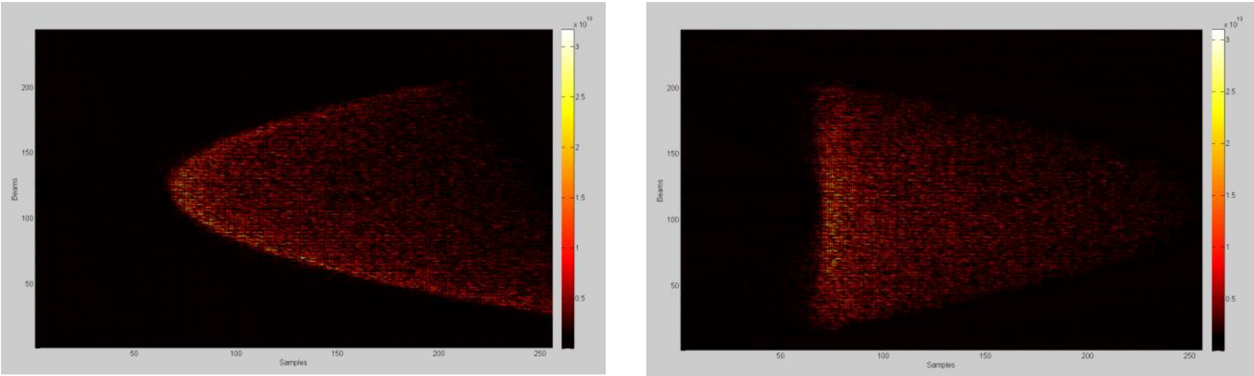

Figure 21. Stack without (left) and with (right) geometry corrections applied.

Although in CryoSat-2 and Sentinel-3 these corrections have been applied separately and in different steps and domains (in the case of the slant range correction), we intend to apply them all together and in the same domain, before the range compression is performed. Thus, all the corrections will be applied as a phase shift and with no need to be split into coarse and fine corrections.

Range compression

This algorithm performs a range compression of the waveforms. That is, the conversion of each Doppler beam of a stack to the frequency domain. This is done with an FFT in the across-track direction. Due to data rate volume limitations, the FFT is normally performed with a zero-padding factor of 1, or maximum 2. An FFT with a zero-padding factor is theoretically the best possible interpolation, because it uses the phase information, as it is performed with the video signals before the waveform power computation.

Multi-looking

This algorithm computes the non-coherent summation of all the power beams corresponding to each surface location. This means that, for each stack, the beams have been squared (hence, phase information has been lost) and, after that, averaged. The result of this operation is a L1B waveform per stack.

Additionally, before averaging all the beams from the stack, another process is carried out. In order to compute the stack characterisation parameters for the L1B product, a smoothing is performed so as to have a better fitting of the stack. This smoothing process is called sub-stacking. Note that this process is only applied for characterisation of the stack and it is not applied to the waveforms.

Sigma-0 scaling factor

This algorithm computes the Sigma-0 scaling factor that is used at Level 2 to determine the backscatter coefficient of the surface from which the echoes have been reflected. The Sigma-0 scaling factor is based on the radar equation, which indicates the power relationship between the echoes transmitted and received considering a single beam.

That concludes the description of the Delay-Doppler processing concept and the steps required to generate L1b SAR waveforms. In the next section we provide an overview of the retracking algorithms that have, to date, been applied to SAR L1b data.

4.3. Overview of SAR Retracking

The enhanced resolution provided by the new altimetric mode, also known as the SAR mode, compared to conventional altimetry mode or Low Resolution Mode (LRM), offers a unique opportunity to better understand and characterise ice sheets, especially at the margins and where topographic features are present.

However, the wide variety of scenarios over ice sheets results in a large variety of echo shapes. These may include both single- and multi-peak echoes, and those which are from more specular or diffuse scattering. In general, waveforms may be classified according to their shape, for example into ocean-like, leads-like or very specular and multi-peak. Provided the new nature of these observed waveforms we need a waveform model flexible and adaptable to these shapes. Having a unique model for all shapes is unlikely to happen, but investigations done by one of the teams within this consortium (isardSAT) [*Martin-Puig and García*, 2013] have shown that the SAMOSA solution is very rich for waveform shapes of the first kind (ocean-like). On top of this, recent investigations also showed the capacity of the SAMOSA solution to fit lead-like waveforms, or waveforms of second kind as detailed above [*Jain et al.*, 2014].

The peculiarity of *Ray et al.* [2015] and *Martin-Puig et al.* [2014] is that when deriving the model waveform both accounted for Barrick's work on rough surface scattering based on specular point theory [*Barrick*, 1968]. This did not consider the radar cross section as a constant value as done in preceding derivations [*Brown*, 1977]. Barrick's definition under Gaussian assumption is given by:

$$\sigma(\theta) \approx \sigma_0(0)\exp\left(-\frac{\tan^2\theta}{\sigma_s}\right)$$

where θ is the incident angle, and σ_s is related to the roughness of the surface under observation. Figure 22 shows the variation in Barrick's radar cross-section as a function of σ_s. Later in 1977 [*Valenzuela*, 1977] related σ_s to the total variance of slopes. After this, other investigators have proven that, in the case of ocean surfaces, σ_s is indeed linked to wind speed [*Liu et al.*, 2000].

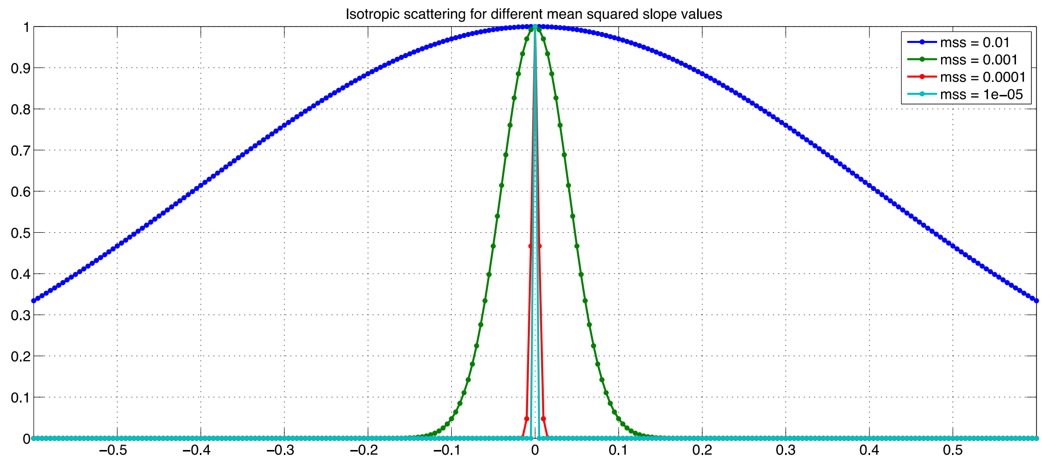

Figure 22. Graphical representation of Barrick's radar cross section for different σ_s.

As shown by *Martin-Puig and García* [2013] without presence of land contamination, e.g. a large lake, the response from the lake is similar, but not the same as the response from the ocean even for small significant wave heights. Over lakes the shape of the echo is peakier as shown in Figure 23.

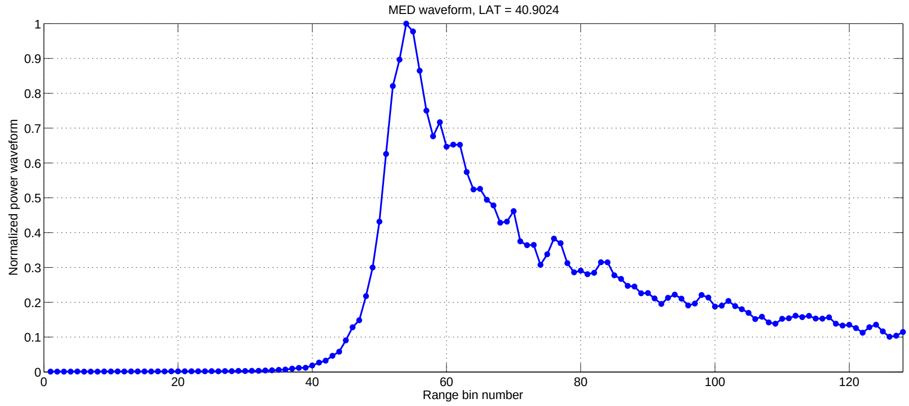

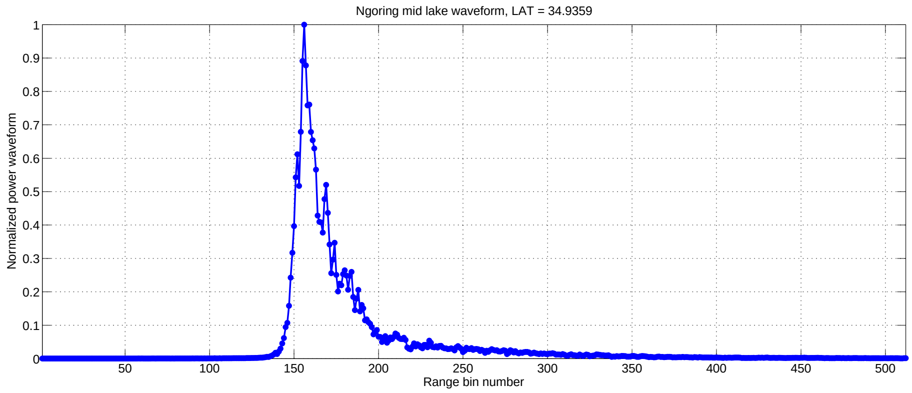

Figure 23. Comparison of ocean backscatter (top) and a lake backscatter (bottom) in SAR and SARin modes of the CryoSat-2 mission.

Note that CryoSat-2 Baseline-B includes zero padding in both SAR and SARin processing chains, thus the sampling space in both images is the same. While the ocean response tail extends for ~ 80 samples or even more, the lake response is more specular and the tail decays rapidly in the next fifty samples after lake level is reached.

We achieve the fitting of the more specular waveform by modifying our fitting approach: instead of fitting for SWH we do fit for roughness (σ_s) by setting the SWH to a small value quasi equal to zero (Figure 24).

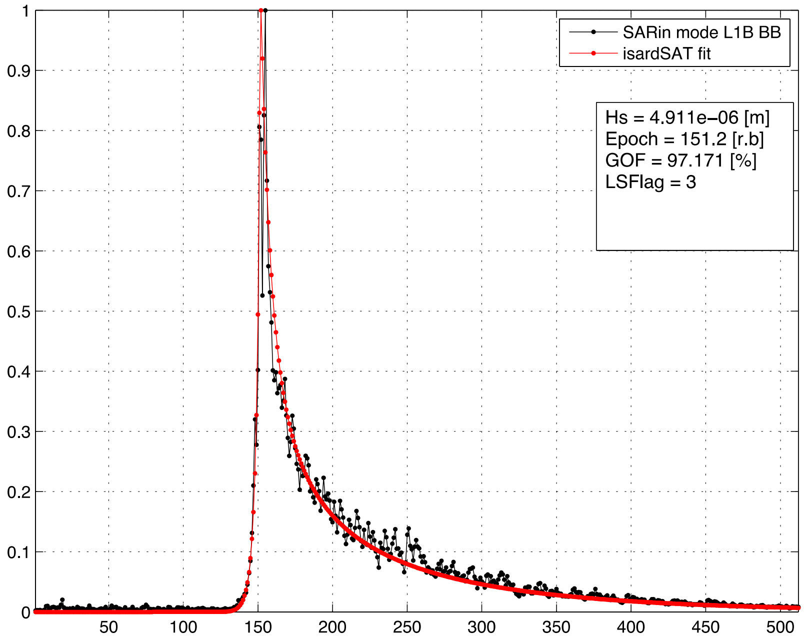

Figure 24. Comparison of model and fitted backscatter using the model of Ray et al. [2014].

This solution allows us to even fit very specular echoes like leads, as shown in Figure 25. Investigation is now needed to assess its performance fitting ice sheet echoes.

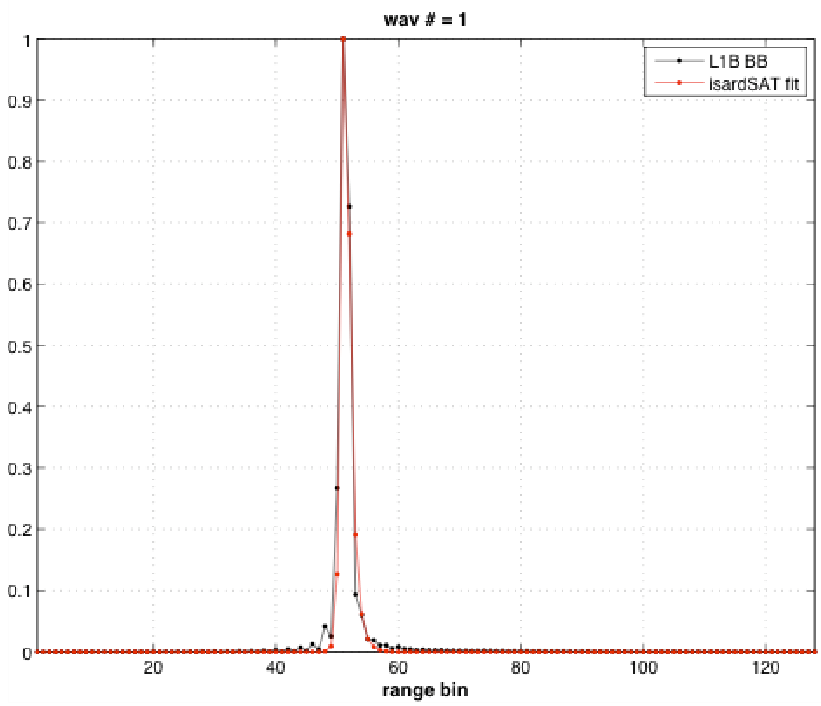

Figure 25. Example of 'lead-like' fitted waveform.

Multiple peak detection of totally distorted waveforms will be difficult to retrack with a model like SAMOSA. Instead, empirical solutions, stack processing techniques, or other techniques based on Level 1 data (e.g. along-track coherence by the use of the temporal information) preceding retracking are needed, in order to eliminate undesired effects, and to help choosing the correct surface reflection (e.g. from close to nadir). These methods represent novel approaches within the field of altimetry retracking over ice sheets, which will be investigated for the first time during the SPICE project. Details of the techniques proposed in this study are provided in the Requirements Baseline document.

5. Recommendations for the SPICE Project

Based upon this scientific review, we have identified the following high-level objectives which serve as recommendations for the SPICE project. These recommendations aim to address some of the key challenges that currently affect radar altimetry observation of ice sheets, with a specific focus on Delay-Doppler, or SAR, altimeter techniques. As such, taken together they fulfil the overall aim of SPICE, which is to establish a robust methodological basis for the development of operational SAR altimetry over the polar ice sheets. Further details relating to their implementation are given within the Requirements Baseline document. The recommended objectives are as follows:

1. Assess and optimise Delay-Doppler altimeter processing for ice sheets.
2. Assess and improve SAR retracker performance over ice sheets.
3. Evaluate the performance of SAR altimetry relative to conventional altimetry.
4. Assess the impact on SAR altimeter measurements of radar wave interaction with the snowpack.

6. References

Arthern, R. J., D. J. Wingham, and A. L. Ridout (2001), Controls on ERS altimeter measurements over ice sheets: Footprint-scale topography, backscatter fluctuations, and the dependence of microwave penetration depth on saetllite orientation, *J. Geophys. Res.*, *106*(D24), 33,471–33,484.

Bamber, J. L. (1994), Ice sheet altimeter processing scheme, *Int. J. Remote Sens.*, *15*(4), 925–938, doi:10.1080/01431169408954125.

Barrick, D. (1968), Rough Surface Scattering Based on the Specular Point Theory, *IEEE Trans. Antennas Propag.*, *16*, 449–454.

Bindoff, N. et al. (2013), Detection and Attribution of Climate Change: from Global to Regional, in *Climate Change 2013: The Physical Science Basis. Contribution of Working Group I to the Fifth Assessment Report of the Intergovenermnetal Panel on Climate Change*, pp. 867–952, Cambridge University Press, Cambridge, UK.

Boening, C., M. Lebsock, F. Landerer, and G. Stephens (2012), Snowfall-driven mass change on the East Antarctic ice sheet, *Geophys. Res. Lett.*, *39*, L21501, doi:10.1029/2012GL053316.

Brenner, A. C., R. A. Blndschadler, R. H. Thomas, and H. J. Zwally (1983), Slope-induced errors in radar altimetry over continental ice sheets, *J. Geophys. Res.*, *88*(C3), 1617, doi:10.1029/JC088iC03p01617.

van den Broeke, M. R., J. Bamber, J. T. M. Lenaerts, and E. Rignot (2011), Ice Sheets and Sea Level: Thinking Outside the Box, *Surv. Geophys.*, *32*, 495–505, doi:10.1007/s10712-011-9137-z.

van den Broeke, M., J. Bamber, J. Ettema, E. Rignot, E. Schrama, W. J. van de Berg, E. van Meijgaard, I. Velicogna, and B. Wouters (2009), Partitioning recent Greenland mass loss., *Science (80-.).*, *326*(5955), 984–6, doi:10.1126/science.1178176.

Brown, G. (1977), The average impulse response of a rough surface and its applications, *IEEE Trans. Antennas Propag.*, *25*(1), 67–74, doi:10.1109/TAP.1977.1141536.

Church, J. A. et al. (2013), Sea Level Change, in *Climate Change 2013: The Physical Science Basis. Contribution of Working Group I to the Fifth Assessment Report of the Intergovernmental Panel on Climate Change*, edited by V. B. and P. M. M. (eds.). Stocker, T.F., D. Qin, G.-K. Plattner, M. Tignor, S.K. Allen, J. Boschung, A. Nauels, Y. Xia, Cambridge University Press, Cambridge, UK.

Cook, A. J., and D. G. Vaughan (2010), Overview of areal changes of the ice shelves on the Antarctic Peninsula over the past 50 years, *Cryosph.*, *4*(1), 77–98.

Davis, C. H. (1997), A Robust Threshold Retracking Algorithm for Measuring Ice-Sheet Surface Elevation Change from Satellite Radar Altimeters, *IEEE Trans. Geosci. Remote Sens.*, *35*(4), 974–979.

Davis, C. H., and R. K. Moore (1993), A combined surface- and volume-scattering model for ice-sheet radar altimetry, *J. Glaciol.*, *39*(133), 675–686.

Davis, C. H., S. Member, and A. C. Ferguson (2004), Elevation Change of the Antarctic Ice Sheet , Radar Altimetry, *IEEE Trans. Geosci. Remote Sens.*, *42*(11), 1995–2000.

Davis, C. H., Y. H. Li, J. R. McConnell, M. M. Frey, and E. Hanna (2005), Snowfall-driven growth in East Antarctic ice sheet mitigates recent sea-level rise, *Science (80-.).*, *308*(5730), 1898–1901, doi:10.1126/science.1110662.

Davis, H. (1995), Growth of the Greenland Ice Sheet: A Performance Assessment of Altimeter Retracking Algorithms, *IEEE Trans. Geosci. Remote Sens.*, *33*(5).

Fettweis, X., G. Mabille, M. Erpicum, S. Nicolay, and M. R. van den Broeke (2011), The 1958–2009 Greenland ice sheet surface melt and the mid-tropospheric atmospheric circulation, *Clim. Dyn.*, *36*, 139–159, doi:10.1007/s00382-010-0772-8.

Flament, T., and F. Rémy (2012), Dynamic thinning of Antarctic glaciers from along-track repeat radar altimetry, *J. Glaciol.*, *58*(211), 830–840, doi:10.3189/2012JoG11J118.

Ford, P. G., and G. H. Pettengill (1992), Venus topography and kilometer-scale slopes, *J. Geophys. Res.*, *97*(E8), 13103, doi:10.1029/92JE01085.

Fu, L., and A. Cazenave (2001), *Satellite Altimetry and Earth Sciences*, Academic Press, San Diego.

Gray, L., D. Burgess, L. Copland, M. N. Demuth, T. Dunse, K. Langley, and T. V. Schuler (2015), CryoSat-2 delivers monthly and inter-annual surface elevation change for Arctic ice caps, *Cryosph. Discuss.*, *9*(3), 2821–2865, doi:10.5194/tcd-9-2821-2015.

Hanna, E., P. Huybrechts, K. Steffen, J. Cappelen, R. Huff, C. Shuman, T. Irvine-Fynn, S. Wise, and M. Griffiths (2008), Increased runoff from melt from the Greenland Ice Sheet: A response to global warming, *J. Clim.*, *21*(2), 331–341, doi:10.1175/2007JCLI1964.1.

Hayne, G. (1980), Radar altimeter mean return waveforms from near-normal-incidence ocean surface scattering, *IEEE Trans. Antennas Propag.*, *28*(5), 687–692, doi:10.1109/TAP.1980.1142398.

Helm, V., a. Humbert, and H. Miller (2014), Elevation and elevation change of Greenland and Antarctica derived from CryoSat-2, *Cryosph.*, *8*(4), 1539–1559, doi:10.5194/tc-8-1539-2014.

Holland, D. M., R. H. Thomas, B. D. E. Young, M. H. Ribergaard, and B. Lyberth (2008), Acceleration of Jakobshavn Isbræ triggered by warm subsurface ocean waters, *Nat. Geosci.*, *1*, doi:10.1038/ngeoXXXX.

Humbert, A., D. Gross, R. M. Uller, M. R. van den Broeke, D. G. Vaughan, and W. J. van de Berg (2010), Deformation and failure of the ice bridge on the Wilkins Ice Shelf , Antarctica, *Ann. Glaciol.*, *51*(55), 49–55.

Hurkmans, R. T. W. L., J. L. Bamber, and J. a. Griggs (2012), Brief communication: “Importance of slope-induced error correction in volume change estimates from radar altimetry,” *Cryospherecryosph.*, *6*, 447–451, doi:10.5194/tc-6-447-2012.

Jain, M., C. Martin-Puig, O. Andersen, L. Stenseng, and J. Dall (2014), EVALUATION OF SAMOSA3 ADAPTED RETRACKER USING CRYOSAT-2 SAR ALTIMETRY DATA OVER THE ARCTIC OCEAN, in *IEEE International Symposium on Geoscience and Remote Sensing IGARSS*.

Joughin, B. E. Smith, and D. M. Holland (2010), Sensitivity of 21st century sea level to ocean-induced thinning of Pine Island Glacier, Antarctica, *Geophys. Res. Lett.*, *37*, L20502, doi:10.1029/2010GL044819.

Joughin, I., R. B. Alley, and D. Holland (2012), Ice-Sheet Response to Oceanic Forcing, *Science (80-.).*, *338*, 1172, doi:10.1126/science.1226481.

Khvorostovsky, K. S. (2012), Merging and Analysis of Elevation Time Series Over Greenland Ice Sheet From

Satellite Radar Altimetry, *IEEE Trans. Geosci. Remote Sens.*, *50*(1), 23–36.

Legresy, B., and F. R. Remy (1997), Altimetric observations of surface characteristics of the Antarctic ice sheet, *J. Glaciol.*, *43*(144), 1–11.

Legresy, B., F. Papa, F. Remy, G. Vinay, M. van den Bosch, and O.-Z. Zanife (2005), ENVISAT radar altimeter measurements over continental surfaces and ice caps using the ICE-2 retracking algorithm, *Remote Sens. Environ.*, *95*(2), 150–163, doi:10.1016/j.rse.2004.11.018.

Lenaerts, J. T. M., E. Van Meijgaard, M. R. Van Den Broeke, S. R. M. Ligtenberg, M. Horwath, and E. Isaksson (2013), Recent snowfall anomalies in Dronning Maud Land, East Antarctica, in a historical and future climate perspective, *Geophys. Res. Lett.*, *40*, 2684–2688, doi:10.1002/grl.50559.

Liu, Y., M.-Y. Su, X.-H. Y. And, and W. T. Liu (2000), The Mean-Square Slope of Ocean Surface Waves and Its Effects on Radar Backscatter, *J. Atmos. Ocean. Technol.*, *17*, 1092–1105.

Martin, T. V., H. J. Zwally, A. C. Brenner, and R. A. Bindschadler (1983), Analysis and retracking of continental ice sheet radar altimeter waveforms, *J. Geophys. Res.*, *88*(C3), 1608, doi:10.1029/JC088iC03p01608.

Martin-Puig, C., and P. García (2013), Synthetic Aperture Radar (SAR) altimetry for hydrology, in *ESA Living Planets Symposium, Edinburgh, Scotland*.

Martin-Puig, C., M. Roca, C. Ray, R. Escolà, and A. García-Mondéjar (2014), A new SAR altimetry waveform model ready for current and forthcoming SAR missions, in *OSTS2014. Konstanz, Germany*.

Martinson, D. G., S. E. Stammerjohn, R. A. Iannuzzi, R. C. Smith, and M. Vernet (2008), Western Antarctic Peninsula physical oceanography and spatio–temporal variability, *Deep. Res. II*, *55*, 1964–1987, doi:10.1016/j.dsr2.2008.04.038.

McMillan, M., H. Corr, A. Shepherd, A. Ridout, S. Laxon, and R. Cullen (2013), Three-dimensional mapping by CryoSat-2 of subglacial lake volume changes, *Geophys. Res. Lett.*, *40*(16), 4321–4327, doi:10.1002/grl.50689.

McMillan, M., A. Shepherd, A. Sundal, K. Briggs, A. Muir, A. Ridout, A. Hogg, and D. Wingham (2014), Increased ice losses from Antarctica detected by CryoSat-2, *Geophys. Res. Lett.*, *41*, 1–7, doi:10.1002/2014GL060111.Received.

Moholdt, G., C. Nuth, J. O. Hagen, and J. Kohler (2010), Recent elevation changes of Svalbard glaciers derived from ICESat laser altimetry, *Remote Sens. Environ.*, *114*(11), 2756–2767, doi:10.1016/j.rse.2010.06.008.

Mouginot, J., E. Rignot, and B. Scheuchl (2014), Sustained increase in ice discharge from the Amundsen Sea Embayment, West Antarctica, from 1973 to 2013, *Geophys. Res. Lett.*, *41*, doi:10.1002/2013GL059069.1.

Nilsson, J. et al. (2015), Greenland 2012 melt event effects on CryoSat-2 radar altimetry, *Geophys. Res. Lett.*, *42*(10), 3919–3926, doi:10.1002/2015GL063296.

Park, J. W., N. Gourmelen, A. Shepherd, S. W. Kim, D. G. Vaughan, and D. J. Wingham (2013), Sustained retreat of the Pine Island Glacier, *Geophys. Res. Lett.*, *40*, 1–6, doi:10.1002/grl.50379.

Pritchard, H. D., R. J. Arthern, D. G. Vaughan, and L. A. Edwards (2009), Extensive dynamic thinning on the margins of the Greenland and Antarctic ice sheets, *Nature*, *461*(7266), 971–975, doi:10.1038/nature08471.

Pritchard, H. D., S. R. M. Ligtenberg, H. A. Fricker, D. G. Vaughan, M. R. van den Broeke, and L. Padman (2012), Antarctic ice-sheet loss driven by basal melting of ice shelves, *Nature*, *484*(7395), 502–505, doi:10.1038/nature10968.

Raney, K. (1998), The delay/doppler radar altimeter, *IEEE Trans. Geosci. Remote Sens.*, *36*(5), 1578–1588, doi:10.1109/36.718861.

Ray, C., C. Martin-Puig, M. P. Clarizia, G. Ruffini, S. Dinardo, C. Gommenginger, and J. Benveniste (2015), SAR Altimeter Backscattered Waveform Model, *IEEE Trans. Geosci. Remote Sens.*, *53*(2), 911–919, doi:10.1109/TGRS.2014.2330423.

Remy, F., P. Mazzega, S. Houry, C. Brossier, and J. F. Minster (1989), Mapping of the Topography of Continental Ice by Inversion of Satellite-Altimeter Data, *J. Glaciol.*, *35*(119), 98–107, doi:10.3189/002214389793701419.

Remy, F., Legresy, and L. Testut (2001), Ice sheet and satellite altimetry, *Surv. Geophys.*, *22*(Figure 2), 1–29.

Remy, F., T. Flament, F. Blarel, and J. Benveniste (2012), Radar altimetry measurements over antarctic ice sheet: A focus on antenna polarization and change in backscatter problems, *Adv. Sp. Res.*, *50*(8), 998–1006, doi:10.1016/j.asr.2012.04.003.

Ridley, J. K., and K. C. Partington (1988), A model of satellite radar altimeter return from ice sheets, *Int. J. Remote Sens.*, *9*(4), 601–624, doi:10.1080/01431168808954881.

Rignot, E. (1998), Fast recession of a West Antarctic glacier, *Science (80-.).*, *281*(5376), 549–551.

Rignot, E., and R. H. Thomas (2002), Mass balance of polar ice sheets, *Science (80-.).*, *297*(5586), 1502–1506.

Rignot, E., G. Casassa, P. Gogineni, W. Krabill, A. Rivera, and R. Thomas (2004), Accelerated ice discharge from the Antarctic Peninsula following the collapse of Larsen B ice shelf, *Geophys. Res. Lett.*, *31*, L18401, doi:L18401 10.1029/2004gl020697.

Rignot, E., G. Casassa, S. Gogineni, P. Kanagaratnam, W. Krabill, H. Pritchard, A. Rivera, R. Thomas, J. Turner, and D. Vaughan (2005), Recent ice loss from the Fleming and other glaciers, Wordie Bay, West Antarctic Peninsula, *Geophys. Res. Lett.*, *32*, L07502, doi:L07502 10.1029/2004gl021947.

Rignot, E., M. Koppes, and I. Velicogna (2010), Rapid submarine melting of the calving faces of West Greenland glaciers, *Nat. Geosci.*, *3*, 187–191, doi:10.1038/ngeo765.

Rignot, E., I. Velicogna, M. R. van den Broeke, A. Monaghan, and J. Lenaerts (2011), Acceleration of the contribution of the Greenland and Antarctic ice sheets to sea level rise, *Geophys. Res. Lett.*, *38*, doi:10.1029/2011GL046583.

Rignot, E., J. Mouginot, M. Morlighem, H. Seroussi, and B. Scheuchl (2014), Widespread, rapid grounding line retreat of Pine Island, Thwaites, Smith, and Kohler glaciers, West Antarctica, from 1992 to 2011, *Geophys. Res. Lett.*, *41*, 3502–3509, doi:10.1002/2014GL060140.Received.

Robertson, R., M. Visbeck, A. L. Gordon, and E. Fahrbach (2002), Long-term temperature trends in the deep waters of the Weddell Sea, *Deep. Res. II*, *49*, 4791–4806.

Robin, G. de Q. (1966), MAPPING THE ANTARCTIC ICE SHEET BY SATELLITE ALTIMETRY, *Can. J. Earth Sci.*, *3*(6).

Roemer, S., B. Legrésy, M. Horwath, and R. Dietrich (2007), Refined analysis of radar altimetry data applied to the region of the subglacial Lake Vostok/Antarctica, *Remote Sens. Environ.*, *106*(3), 269–284, doi:10.1016/j.rse.2006.02.026.

Rott, H., P. Skvarca, and T. Nagler (1996), Rapid collapse of northern Larsen Ice Shelf, Antarctica, *Science (80-.).*, *271*(5250), 788–792.

Rott, H., F. Muller, T. Nagler, and D. Floricioiu (2011), The imbalance of glaciers after disintegration of Larsen-B ice shelf, Antarctic Peninsula, *Cryosph.*, *5*, 125–134, doi:10.5194/tc-5-125-2011.

Scambos, T. A., C. Hulbe, M. Fahnestock, and J. Bohlander (2000), The link between climate warming and break-up of ice shelves in the Antarctic Peninsula, *J. Glaciol.*, *46*(154), 516–530.

Schrama, E. J. O., B. Wouters, and R. Rietbroek (2014), A mascon approach to assess ice sheet and glacier mass balances and their uncertainties from GRACE data, *J. Geophys. Res.*, (February 2003), doi:10.1002/2013JB010923.Received.

Shepherd, A., and D. Wingham (2007), Recent sea-level contributions of the Antarctic and Greenland ice sheets, *Science (80-.).*, *315*(5818), 1529–1532.

Shepherd, A., D. Wingham, and J. Mansley (2002), Inland thinning of the Amundsen Sea sector, West Antarctica, *Geophys. Res. Lett.*, *29*(10), 1364, doi:Artn 1364 Doi 10.1029/2001gl014183.

Shepherd, A., A. Shepherd, D. Wingham, T. Payne, and P. Skvarca (2003), Larsen Ice Shelf Has Progressively Thinned, *Science (80-.).*, *302*(856), 856–859, doi:10.1126/science.1089768.

Shepherd, A., D. Wingham, D. Wallis, K. Giles, S. Laxon, and A. V Sundal (2010), Recent loss of floating ice and the consequent sea level contribution, *Geophys. Res. Lett.*, *37*, L13503, doi:L13503 10.1029/2010gl042496.

Shepherd, A. et al. (2012), A reconciled estimate of ice-sheet mass balance., *Science (80-.).*, *338*(6111), 1183–9, doi:10.1126/science.1228102.

Smith, B., H. A. Fricker, I. Joughin, and S. Tulaczyk (2009), An inventory of active subglacial lakes in Antarctica detected by ICESat (2003-2008), *J. Glaciol.*, *55*(192), 573–595.

Turner, J., S. R. Colwell, G. J. Marshall, T. O. M. A. Lachlan-cope, A. M. Carleton, P. D. Jones, V. Lagun, P. A. Reid, and S. Iagovkina (2005), Antarctic Climate Change During the Last 50 Years, *Int. J. Climatol.*, *25*(February), 279–294, doi:10.1002/joc.1130.

Valenzuela, G. (1977), Theories for the interaction of electromagnetic and ocean waves – A review, *Ocean Sci. Div. Nav. Res. Lab. Washingt. D.C. USA*.

Vaughan, D. G. et al. (2013), Observations: Cryosphere., in *Climate Change 2013: Physical Science Basis. Contribution of Working Group I to the Fifth Assessment Report of the Intergovernmental Panel on Climate Change*, edited by V. B. and P. M. M. (eds. . Stocker, T.F., D. Qin, G.-K. Plattner, M. Tignor, S.K. Allen, J. Boschung, A. Nauels, Y. Xia, Cambridge University Press, Cambridge, UK.

Wingham, D., A. Ridout, R. Scharroo, R. Arthern, and C. Shum (1998), Antarctic elevation change from 1992 to 1996, *Science (80-.).*, *282*(5388), 456–458.

Wingham, D. J. (1995), A method for determining the average height of a large topographic ice sheet from observations of the echo received by a satellite altimeter, *J. Glaciol.*, *41*(137), 125–141.

Wingham, D. J. et al. (2006), CryoSat: A mission to determine the fluctuations in Earth's land and marine ice fields, in *NATURAL HAZARDS AND OCEANOGRAPHIC PROCESSES FROM SATELLITE DATA*, vol. 37, edited by M. Singh, RP and Shea, pp. 841–871, ELSEVIER SCIENCE LTD.

Zwally, H. J., M. B. Giovinetto, J. Li, H. G. Cornejo, M. A. Beckley, A. C. Brenner, J. L. Saba, and D. Yi (2005), Mass changes of the Greenland and Antarctic ice sheets and shelves and contributions to sea-level rise : 1992 – 2002, *J. Glaciol.*, *51*(175), 1992–2002.

Zwally, H. J. et al. (2011), Greenland ice sheet mass balance: distribution of increased mass loss with climate warming; 2003–07 versus 1992–2002, *J. Glaciol.*, *57*(201), 88–102, doi:10.3189/002214311795306682.